

# UNCLASSIFIED

AD NUMBER	
AD368068	
CLASSIFICATION CHANGES	
TO:	unclassified
FROM:	confidential
LIMITATION CHANGES	
TO:	Approved for public release, distribution unlimited
FROM:	Distribution: Further dissemination only as directed by Director, Naval Research Laboratory, Washington, DC 20390, 18 NOV 1965, or higher DoD authority.
AUTHORITY	
NRL ltr dtd 17 Sep 2007; NRL ltr dtd 17 Sep 2007	

THIS PAGE IS UNCLASSIFIED

UNCLASSIFIED

AD NUMBER
AD368068
CLASSIFICATION CHANGES
TO
confidential
FROM
secret
AUTHORITY
30 Nov 1977, per document marking, DoDD 5200.10

THIS PAGE IS UNCLASSIFIED

# **SECURITY**

---

# **MARKING**

**The classified or limited status of this report applies to each page, unless otherwise marked.**

**Separate page printouts MUST be marked accordingly.**

---

**THIS DOCUMENT CONTAINS INFORMATION AFFECTING THE NATIONAL DEFENSE OF THE UNITED STATES WITHIN THE MEANING OF THE ESPIONAGE LAWS, TITLE 18, U.S.C., SECTIONS 793 AND 794. THE TRANSMISSION OR THE REVELATION OF ITS CONTENTS IN ANY MANNER TO AN UNAUTHORIZED PERSON IS PROHIBITED BY LAW.**

**NOTICE: When government or other drawings, specifications or other data are used for any purpose other than in connection with a definitely related government procurement operation, the U. S. Government thereby incurs no responsibility, nor any obligation whatsoever; and the fact that the Government may have formulated, furnished, or in any way supplied the said drawings, specifications, or other data is not to be regarded by implication or otherwise as in any manner licensing the holder or any other person or corporation, or conveying any rights or permission to manufacture, use or sell any patented invention that may in any way be related thereto.**

**SECRET**

NRL Report 6371  
Copy No. **1**

368068

**The Spectral Characteristics and Temporal  
Behavior of HF Radar Echoes from  
Over-the-Horizon Aircraft Targets**  
[Unclassified Title]

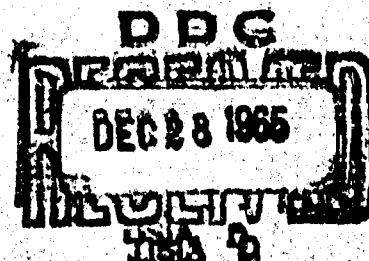
J. R. DAVIS, J. F. THOMASON, J. M. HUDNALL, F. E. BOYD, AND F. H. UTLEY

*Radar Techniques Branch  
Radar Division*

November 18, 1965



**U.S. NAVAL RESEARCH LABORATORY**  
Washington, D.C.



**SECRET**

Downgraded at 12 year intervals;  
Not automatically declassified.

**DDC CONTROL**  
NO. 55736

See inside of cover for distribution restriction.

**SECRET**

**SECURITY**

This document contains information affecting the national defense of the United States within the meaning of the Espionage Laws, Title 18, U.S.C., Sections 793 and 794. The transmission or revelation of its contents in any manner to an unauthorized person is prohibited by law.

In addition to security requirements which apply to this document and must be met, it may be further distributed by the holder *only* with specific prior approval of the Director, U.S. Naval Research Laboratory, Washington, D.C. 20390.

**SECRET**

SECRET

## CONTENTS

Abstract	ii
Problem Status	ii
Authorization	ii
INTRODUCTION	1
The Madre Research Radar	1
NRL Experience in Detecting and Tracking OTH Aircraft Targets	10
The Purpose of This Report	11
TIME-RANGE TRACKING OF OTH AIRCRAFT TARGETS	12
TEMPORAL VARIATIONS IN SIGNAL STRENGTH OF OTH AIRCRAFT RADAR ECHOES	22
THE SPECTRAL CHARACTERISTICS OF OTH AIRCRAFT RADAR ECHOES	44
CONCLUSIONS	49
REFERENCES	53
APPENDIX A - Automatic Data-Processing Methods Used for Madre OTH Aircraft Observations	55
APPENDIX B - Selection of Most Probable Ionospheric Path	59
DISTRIBUTION	61

SECRET

SECRET

ABSTRACT  
[Secret]

This report summarizes the results of three years of over-the-horizon (OTH) radar tracking studies conducted at NRL. The purpose of these studies was to investigate the feasibility and reliability of utilizing ionospheric propagation paths as a means of extending radar usefulness to ranges beyond the geometric horizon. The principal instrument used in these studies was the Madre research radar, which is a high-power, coherent, moving-target-indicating (MTI) radar operating in the high-frequency portion of the radio spectrum.

Detailed analyses of the following three phases of the OTH aircraft target study were made: (a) aircraft time-range tracking, (b) temporal behavior of the aircraft target echo, and (c) spectral characteristics of the aircraft target echo. The essential results are, respectively: (a) a range measurement accuracy of approximately 5 percent may be expected under usual conditions, even if no effort is made to correct the raw slant-range data for the effects of ionospheric path; (b) a typical OTH target can normally be acquired 60 percent of the time during which it is illuminated, compared to a 6 percent acquisition rate for noncoherent radars; and (c) the number of aircraft in a closely spaced group of aircraft can be determined and separated in velocity with a doppler resolution of at least 1/10 cps.

PROBLEM STATUS

This is an interim report; work on the problem is continuing.

AUTHORIZATION

NRL Problem R02-42  
Project MIPR (30-602) 64-3412

Manuscript submitted November 3, 1965.

SECRET

SECRET

THE SPECTRAL CHARACTERISTICS AND TEMPORAL  
BEHAVIOR OF HF RADAR ECHOES FROM OVER-THE-HORIZON  
AIRCRAFT TARGETS  
[Unclassified Title]

INTRODUCTION

The Madre Research Radar

The Madre research radar is a high-power, coherent, moving-target-indicating (MTI) radar which operates in the high-frequency (hf) portion of the radio spectrum. It has been developed by NRL as a tool for investigating the feasibility of utilizing ionospheric propagation paths as a means of extending radar usefulness to ranges beyond the geometric horizon. In view of the unique circumstances which pervade the introduction of radar techniques into an environment previously of concern only to communicators, a brief description of the parameters of the Madre radar and the rationale behind their selection follows.

The range interval in which targets may be illuminated by a radar which exploits ionospheric propagation to transmit energy beyond the horizon extends to more than 2200 naut mi (for single-hop propagation) from the radar site. The extreme range is greatly extended if multiple-hop propagation is utilized, although the difficulties of achieving reliable extended geographical coverage with multiple-hop propagation are considerable. The detection of radar targets such as aircraft at ranges of 2000 naut mi, and farther, absolutely requires that the observer make use of all the means available to him for maximizing the radar's sensitivity to these targets. The selection of operating frequency and vertical radiation angle to insure optimum utilization of the propagation medium are important considerations in the operation of an hf radar, but they should probably be treated as techniques rather than as true tools and should be made available to the operator by providing the widest possible flexibility in the radar itself. The actual radar parameters which are under control of the designer and can be described as being tools, are most adequately expressed by the radar equation

$$\frac{P_r}{P_n} = \frac{P_t G_t G_r \lambda^2 L}{(4\pi)^3 R^4 P_n} \sigma,$$

where

- $P_r$  = received signal power,
- $P_n$  = received noise power within the receiver bandwidth,
- $P_t$  = transmitted power,
- $G_t$  = effective gain of antenna for transmitting,
- $G_r$  = effective gain of antenna for receiving,
- $\lambda$  = wavelength,
- $R$  = range to target,

SECRET



$\sigma$  = target echoing cross section, and

$L$  = miscellaneous losses (including ionospheric transmission loss as the principal constituent).

This equation is best applied to the Madre radar in its average-power version:

$$\frac{\bar{P}_r}{P_n} = \frac{\bar{P}_t G_t G_r T_f \lambda^2 L}{(4\pi)^3 R^4 p_n} \sigma,$$

where  $p_n$  is the received noise power per cps, the horizontal bars over quantities indicate average values, and  $T_f$  is the coherent integration time or the reciprocal of the final predetection filter bandwidth (they will normally be the same for a properly designed signal processor).

The factor  $L$  may be manipulated slightly by a proper selection of transmitting frequencies, within the flexibility of the radar, to bring about optimum illumination of the target region. The factors  $\bar{P}_t$ ,  $G_t$ ,  $G_r$ , and  $T_f$ , however, are of primary importance in determining the performance of an hf radar.  $\bar{P}_t$  was largely determined for the Madre research radar by the state of the hf-transmitter art. A 100-kilowatt (kw) average power (4.6 megawatt (Mw) peak power) transmitter was constructed which possesses adequate flexibility for operation in the full 10- to 30-Mc/s frequency band at a variety of pulse shapes and pulse repetition frequencies (prf's).

Selection of the other parameters was based in large part upon environmental factors. For efficient use of the transmitted energy,  $G_t$  was chosen to be equal to  $G_r$ , and a single antenna was constructed with a duplexer to be utilized both for transmission and for reception. The expense of constructing a large array, capable of accepting high power levels and flexible enough to cover a diversity of geographic regions over a wide operating bandwidth, imposed an upper limit on the antenna gain which it was believed could be achieved. The dichotomous objectives of covering an extended range interval and, at the same time, providing high gain could have been met by constructing a single beam which could be steered in elevation. This option was excessive in cost, so a lobed vertical structure was chosen. The azimuthal beamwidth was selected to permit steering over an arc of approximately 60 degrees without serious pattern degradation and also to be broad enough so that the possibility of ionosphere-generated azimuthal path deviations of a few degrees would not seriously impair an operator's confidence in knowing the region of coverage. Principal lobe half-power beamwidths were selected which vary between 8 and 14 degrees in azimuth and between 3 and 7 degrees in elevation over the 13.5- to 27-Mc/s frequency band. A plot of effective antenna gain (including an assumed 6-db enhancement due to constructive ground interference at lobe peaks vs frequency appears in Fig. 1. The requirement for a diversity of vertical takeoff angles to be used under the widely varying demands of the ionospheric path was met by utilizing two vertically stacked rows of radiating elements in corner reflectors. These elements provide elevation coverage between 1.75 and approximately 30 degrees in several lobes selectable by appropriate phasing and choice of operating frequency. Figure 2 is a photograph of the Madre phased antenna array showing also an elevated rotatable corner reflector which is used in studying ballistic missile launches to the south and west.

The coherent integration time, or final predetection filter bandwidth, was selected in keeping with the expected doppler frequency stability of constant-velocity aircraft target echoes received over the ionospheric path. A value of 10 sec for the integration time (or 1/10-cps filter bandwidth) was selected to exploit this expected doppler frequency stability.

Fig. 1 - Effective antenna gain vs frequency for the Madre high-frequency broadside array

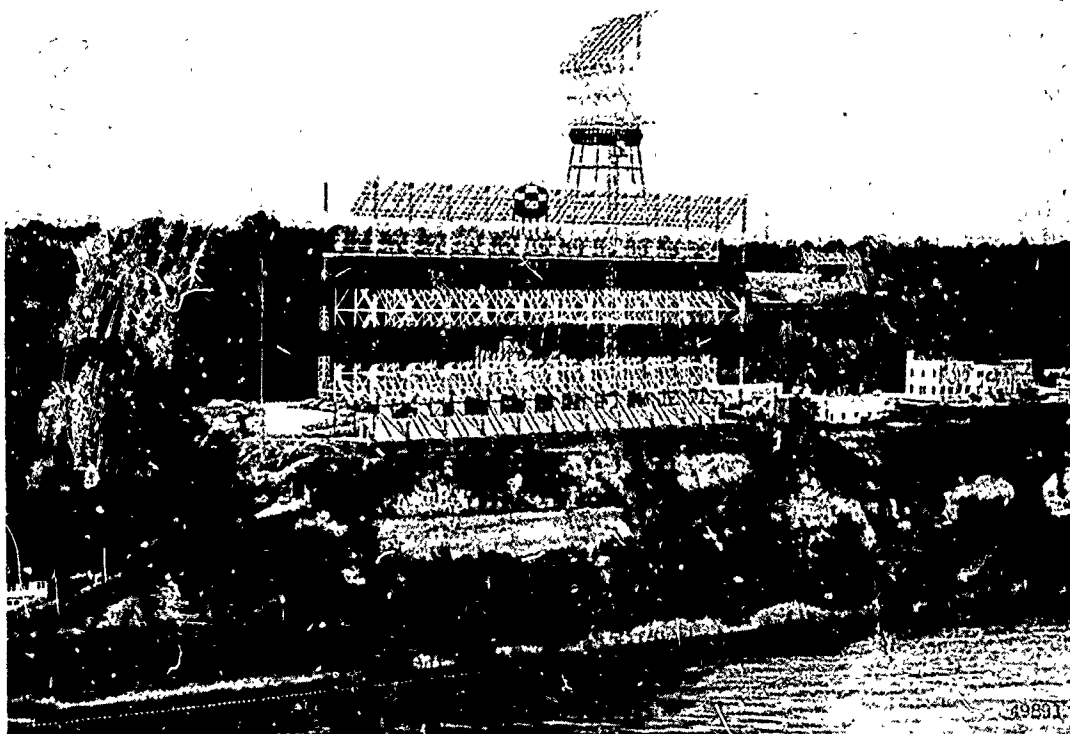
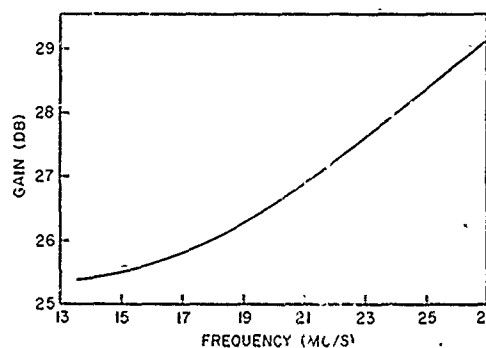


Fig. 2 - The Madre high-frequency broadside array and an elevated rotatable corner reflector

The coherent integration or bandwidth narrowing process is accomplished in the Madre radar with the use of a rotating magnetic drum for storage of the range-gated, bipolar, video echo information which is impressed upon it. Received signals are gated into 23 range gates of approximately 20 naut mi width and are stored on the drum in separable locations for 20 sec. Stored information is continuously renewed, with the latest 20 sec of information being always available for reading out of storage. The readout process is accomplished by a single scanning doppler filter whose effective bandwidth is 1/10 cps. This filter scans across 10-cps segments of the doppler spectrum with a preset sampling period, normally between 1 and 6 sec, sampling all 23 range intervals within this period.

A second filter with a  $1/3$ -cps effective bandwidth is used for a gross picture of the target information and scans across the full doppler spectrum at a preset rate, normally 2.5 sec per scan.

The various radar parameters may be expressed in terms of a figure of merit,  $\bar{P}G_rT_f$ , which, for the Madre radar, may be evaluated as follows:

$$\bar{P} = 100 \text{ kw} = 50 \text{ dbw},$$

$$G_t = G_r = 320 \text{ to } 800 = 25 \text{ to } 29 \text{ db},$$

and

$$T_f = 10 \text{ sec} = 10 \text{ db}.$$

So,  $\bar{P}G_rT_f = 110 \text{ to } 118 \text{ db}$  above 1 w-sec. The 8-db variation occurs across the 13.5- to 27-Mc/s operating bandwidth.

One additional parameter which is contained in the radar equation is also under the observer's control, but it is hidden under the guise of received noise power. External noise, such as cosmic or atmospheric noise, and even man-made noise and co-channel interference are largely not under the observer's control. But the major constituent of the received noise power to which an over-the-horizon (OTH) radar receiver is sensitive is the ground-backscatter signal returning from approximately the same geographic region as target echoes. This energy represents a coherent "effective noise" which must be discriminated against in the receiving or signal processing system in order to render aircraft targets visible. Indeed, the enormous region of ground illuminated at a range of 2000 naut mi by a 20-naut-mi radar pulse transmitter with an antenna beam only 8 degrees in azimuthal extent exceeds the effective radar cross section of an aircraft target by a factor which varies between  $10^4$  and  $10^{10}$ . The MTI technique, utilized with a coherent signal-processing system, makes it possible, however, to filter out most of the large clutter signal. This function is performed in the Madre radar by a series of crystal comb filters which attenuate (by 70 to 80 db) the large clutter signal, whose spectrum is concentrated around the center-frequency and prf-associated harmonics, without degrading moving-target echoes whose doppler shifts exceed a few cycles per second.

Perhaps the clearest expression of the function performed by these backscatter filters is contained in Figs. 3 and 4. Figure 3 contains (a) a sketch of typical illumination geometry for propagation in the 600- to 1200-naut-mi range interval, and (b) two photographs of the clutter-plus-signal echo received from that interval. The amplitude in millivolts (mv) at the antenna terminals appears along the left of each photograph. The upper photograph contains three amplitude vs time delay (approximate range) traces taken at intervals of  $1/60$  sec at a synchronous-detector output location in the receiver with no clutter filtering employed. The lower photograph contains a 5-sec exposure of the same information and shows the tendency of ground backscatter to fill the range interval when viewed over a period of time comparable to the coherent integration period. Figure 4 contains another series of synchronous-detector outputs, of which the top photograph is an unfiltered trace of the type in Fig. 3. The center photograph is a brief exposure of a synchronous-detector trace in which some clutter filtering has been performed and in which an extraordinarily large simulated target signal, masked in all the previous photographs by the enormous clutter echo, has become visible. The bottom photograph contains a smaller, but still extremely large, target echo which is masked by the residual ground backscatter which has penetrated the clutter filters.

It should be evident in Fig. 4 that even an unrealistically large, simulated target echo is difficult to discern in an environment of unfiltered ground backscatter. The degree of clutter rejection employed in the bottom photograph of Fig. 4 is also inadequate (by itself) to render such a target visible.

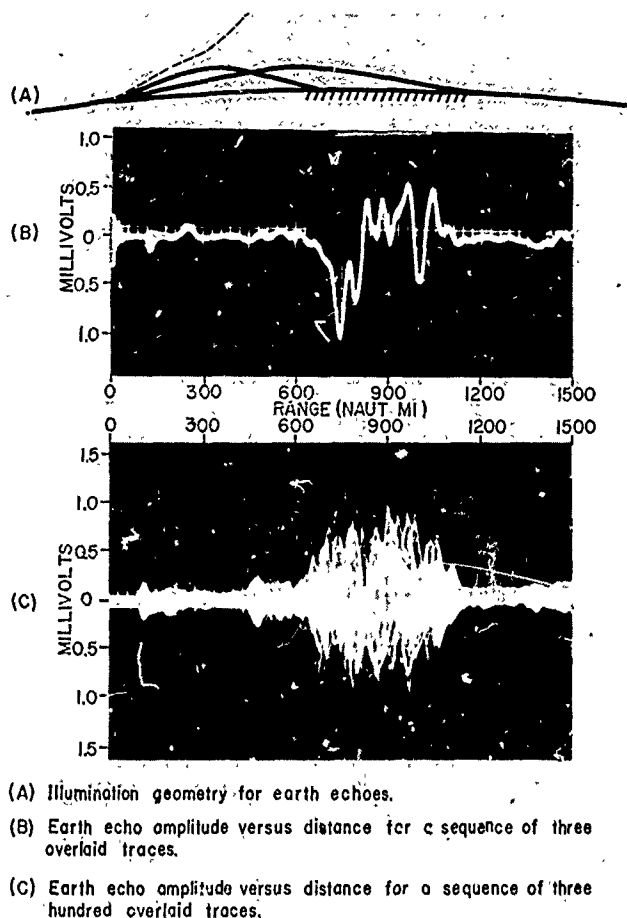
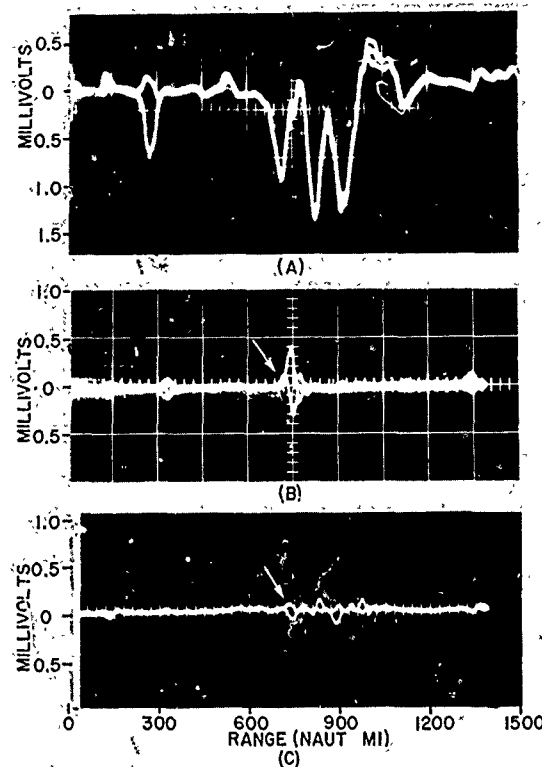


Fig. 3 - Typical ground-backscatter amplitude vs range for the 600- to 1200-naut-mi range interval. No clutter filtering was employed in the Madre synchronous-detector output.

The types of format in which the Madre output information may be presented are widely varied. The normal type of presentation is a velocity (or doppler frequency) vs range format in which output information from the 1/10- or 1/3-cps scanning doppler filter is displayed on a synchronized vertically-swept trace, with range as the horizontal parameter. Signal amplitude appears as intensity modulation in this type of format. Figure 5 is an illustration of the doppler frequency vs range display employed with the 1/3-cps doppler filter. In Fig. 5, the upper photograph is a signal-amplitude vs range trace of a fairly large, clutter-filtered radar echo, similar to the data in Fig. 4. The arrow points to the target location, but the deflection on the A-scope trace at that point is not a target echo. The actual target is thoroughly masked by residual clutter. The center photograph is a doppler vs range display of this target. The bottom photograph is a doppler vs range display of an effective 30-m<sup>2</sup> target in which meteor echoes (the extensive, vertically smeared traces) and external noise are evident. The target echo in this photograph is comparable in amplitude to the meteor echoes and noise traces, but it would be seen to display much more persistent and predictable behavior in both

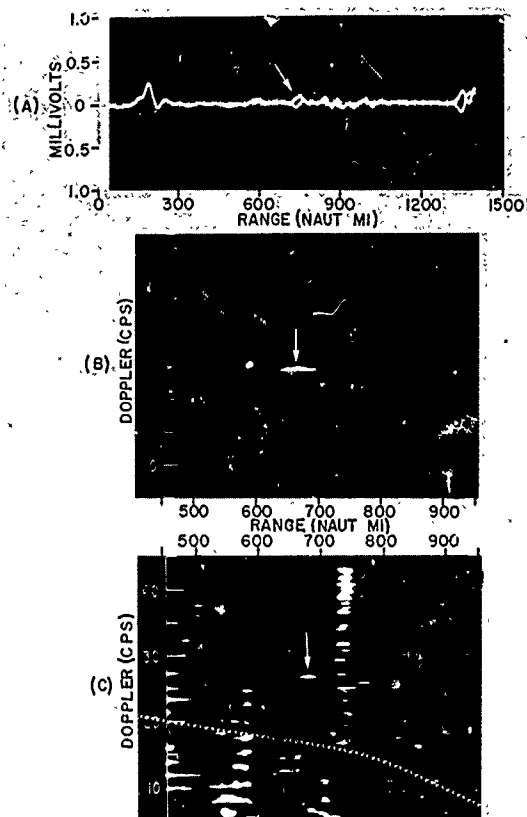


- (A) Three consecutive overlaid traces of earth echo plus meteor echoes at 250 and 1000 nm.
- (B) Three consecutive overlaid traces of clutter-filtered channel with  $3 \times 10^7 \text{ M}^2$  target at 750 nm.
- (C) Three consecutive overlaid traces of clutter-filtered channel with  $3 \times 10^5 \text{ M}^2$  target at 750 nm.

Fig. 4 - Synchronously detected amplitude vs-range for ground-backscatter echoes plus simulated target signal. Some clutter filtering was employed in the Madre synchronous-detector output.

range and doppler frequency over a period of time. Indeed, a criterion upon which most initial target acquisitions are based is the simple rule-of-thumb that a trace must either remain visible at approximately the same range and velocity for substantially longer than the 20-sec signal processor storage period, or the trace must recur repeatedly within a few minutes at approximately the same range and velocity.

It should be emphasized that the series of photographs in Figs. 3 through 5 is not meant to indicate the sizes (in apparent radar cross section) of the targets for which the Madre research radar is intended. Aircraft targets at all ranges are discernible under favorable conditions even during periods when the received signal descends in amplitude to a few tenths of a microvolt peak-to-peak, a value corresponding to an estimated apparent radar cross section of less than  $1 \text{ m}^2$  for a target at 1000 naut mi under the usual operating conditions for the Madre radar.



(A) Clutter filtered zero frequency channel with  $3 \times 10^3 M^2$  target at 750nm.  
 (B) Doppler analysis with 1/3 cps resolution versus range of  $3 \times 10^3 M^2$  target.  
 (C) Doppler analysis with 1/3 cps resolution versus range of  $30 M^2$  target.

Fig. 5 - Clutter-filtered ground backscatter plus simulated target in (a) amplitude vs range and (b and c) doppler frequency vs range formats

A second type of display format is achieved with the use of a doppler - range gate, which may be placed at any location in the doppler vs range display and is useful for a fine-grain examination of selected target echoes. The doppler-range gate, as normally utilized, displays a doppler extent of 1 to 2 cps and a range extent of 100 naut mi. Figure 6 contains examples of the two doppler-range displays. Several remote aircraft targets and a calibration signal trace (upon which a vertical strobe line is visible) appear on the photograph at the upper left. A band of near-range wideband noise also may be seen along the left side of this photograph, which shows the 1/3-cps scanning filter output. The upper right photograph is a doppler-range display of the 1/10-cps filter output in which 10 cps of the doppler extent is shown and in which the calibration signal and the near-range noise appear. The illuminated box at the right in the photograph represents the doppler-range gate and contains the calibration signal at 250 knots and 2050 naut mi in range.

The lower photograph in Fig. 6 is an example of one use to which the doppler-range gate may be readily applied. In this photograph the echo amplitude within the illuminated

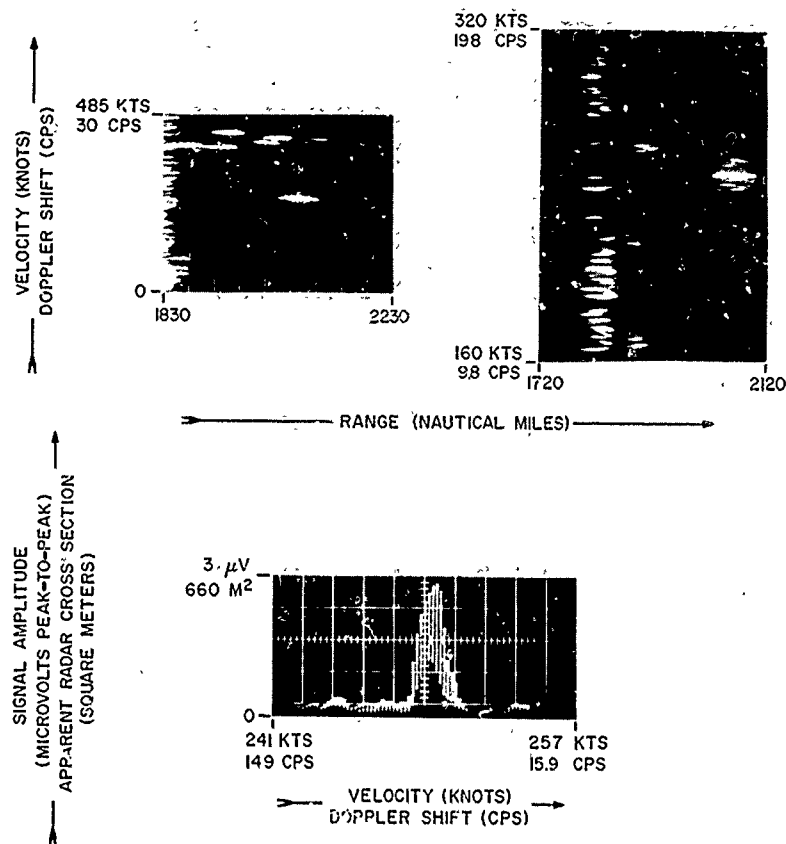


Fig. 6 - Doppler-range displays (top) and spectrum analysis of gated target echo (bottom)

box is displayed versus doppler shift. This display is, in effect, a spectrum analysis of the signal and shows the broadening or dispersion of one of the spectral lines in the pulse spectrum - in general, the dispersion of the doppler shifted carrier. It should be understood that the individual vertical lines in this photograph do not represent actual spectral components, however. They should instead be regarded as closely-spaced samples, whose envelope describes the actual spectral distribution of energy. The spacing of the lines themselves is related to the rate at which the scanning doppler filter is scanned over the 10-cps doppler interval in the photograph at the upper right and has no significance for this discussion. The width of the envelope described by the amplitude samples gives an indication of the signal's stability in doppler shift. In this particular case, in which a stable-frequency calibration signal is shown, the envelope width indicates the actual resolution bandwidth of the 1/10-cps doppler filter.

A second use to which the doppler vs range gate may be applied is in the continuous recording of sampled signal amplitude information. In this application, a peak detector is placed on the doppler-range gate output, and the amplitude data are recorded continuously on chart paper. The scanning doppler filter is normally scanned at a sampling rate of one sample per second for this purpose.

Table 1 contains a listing of the performance parameters with which the Madre radar is normally operated in the aircraft tracking and surveillance modes. A more detailed description of the Madre radar may be found in Refs. 1-5.

Table 1  
Performance Parameters of the Madre Radar

Frequency Band	13.5 - 27.0 Mc/s
Average Power	100 kw
Peak Power	4.6 Mw
Antenna Gain (over an isotrope, including assumed 6-db ground enhancement)	25 - 29 db
Pulse Length (at -20 db points)	250 to 800 $\mu$ sec
Pulse Repetition Frequencies	45, 60, 90, and 180 pps
Storage Time	20 sec
Coherent Integration Times	3 or 10 sec
Final Predetection Filter Bandwidth	1/3 or 1/10 cps

Table 2 contains a listing of the maximum unambiguous radial target velocities, which may be measured with the Madre radar at selected frequencies and pulse rates, and also the maximum apparent unambiguous target ranges which may be measured at these pulse rates. The equivalent velocity resolution afforded by the 1/10-cps doppler filter also is listed.

Table 2  
Maximum Unambiguous Radial Target Velocities and Apparent  
Unambiguous Target Ranges for the Madre Radar

Frequency (mc/s)	Velocity Resolution at 1/10 cps (knot)	Maximum Unambiguous Radial Velocity (knot) at a PRF of			
		45 cps	60 cps	90 cps	180 cps
26.6	1	246	329	493	985
19.3	1.5	340	454	680	1359
13.5	2.2	486	647	971	1940
Maximum (nominal) Unambiguous Range (naut mi)		1800	1350	900	450

It should be mentioned that the true maximum unambiguous range is determined by ionospheric conditions; that is, the ranges from which target echoes actually are received are the ranges to which ionospheric propagation is possible. Because these ranges are known to the operator, and seldom occupy more than 1000 to 1500 naut mi in range extent, he may operate the radar at a prf whose apparent maximum unambiguous range is less than the range in which he is interested without fear of confusing targets at close range with those he is seeking. This circumstance is best expressed in Fig. 7, in which a



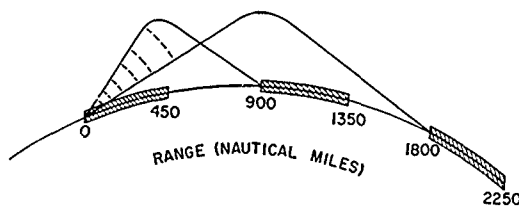


Fig. 7 - Typical ionospheric propagation geometry for OTH observations, showing gated range intervals

hypothetical (but typical) propagation situation is expressed by the rays which begin at the radar site and provide illumination between 900 and 1800 naut mi. At a pulse rate of 90 pps the radar is sensitive unambiguously to 900 naut mi in range. Blanking out the first 450-naut-mi interval and successive odd-numbered intervals, as shown by cross-hatching on Fig. 7, the Madre signal processing system's 23 range gates will be sensitive to over-the-horizon (OTH) target information from only the 1350- to 1800-naut-mi interval, because no propagation paths exist into the 450- to 900-naut-mi range interval. There exists in this case, then, no possibility of confusion due to "around-the-time-base" target echoes. References 6-9 describe a technique which is available for the few occasions in which the illuminated target area cannot be so placed as to remove the range ambiguities by these simple means.

#### NRL Experience in Detecting and Tracking OTH Aircraft Targets

A large body of information has been gathered with the Madre radar during the four-year period that had elapsed since the high-power transmitter and broadside array first became available in 1961. Since the autumn of that year, aircraft surveillance and tracking operations have been conducted as a part of routine system operation under widely varying propagation path conditions. During this time, two classes of aircraft surveillance operations have been conducted and are explained below.

Knowledge of an aircraft's approximate flight path prior to observation is a major advantage in detecting and tracking aircraft, and hence all flights which satisfy this criterion have been grouped into a single class, denoted as Class I. Class I includes (a) "cooperative" and (b) "noncooperative" flights, with the former denoting flights which have been conducted specifically for the Madre radar study, and the latter denoting flights for which a Madre radar study has been only incidental.

A series of 16 military aircraft flights of the Class I cooperative type have been conducted. One of these flights was in fact responsible for the earliest identified over-the-horizon (OTH) aircraft track made with the Madre radar and took place on Sept. 5, 1961. During the series of cooperative aircraft flights, targets have been tracked at distances from 500 to 2200 naut mi, and continuous tracks of over 700 naut mi in length have been obtained. An example of this type of operation is the flight of a Navy P3A Orion from Norfolk, Virginia, to Lajes Air Force Base, Azores, which is discussed in more detail in the next two sections of this report, "Time-Range Tracking of OTH Aircraft Targets," and "Temporal Variations in Signal Strength of OTH Aircraft Radar Echoes."

A number of Class I noncooperative flights have also been tracked. Examples of this type of operation are the Highboy\* operations of the U.S. Marine Corps. This

\*Highboy is a tactical designation for trans-Atlantic aerial refueling missions involving jet fighter aircraft of the Second Marine Aircraft Wing.

report includes, in the next two sections, a detailed account of Madre radar operations in conjunction with Highboy V on May 15, 1964. For both types of Class I operations, Madre radar observations have been confirmed by postflight data from various sources.

A second class of aircraft surveillance by the Madre radar (Class II) involves the surveillance of an area of the North Atlantic Ocean without prior knowledge of particular flight parameters or aircraft population. The target data acquired in this "blindfold" surveillance is later compared with postflight data obtained from appropriate air traffic control centers to determine the effectiveness of the Madre system in this "radar fence" type of operation. The task of separating targets from noise is much more difficult in Class II operations when the exact position of the target is not known, and hence this blindfold surveillance test is believed to be a useful indicator of a potential operational surveillance system's performance. The utility of Class II operations is graphically illustrated when there exists a multiplicity of targets, as is the case for the operations of Oct. 27, 1964, to be discussed in the next two sections of this report.

Also included in Class II are several aircraft targets of opportunity which have been tracked during this period under a variety of operating conditions. Although most of these targets can probably be identified in the same manner as those described above, no attempt has been made to do so. They have been obtained in pursuit of one of the major objectives of the Madre research radar, namely, an investigation of aircraft echo signal behavior under a diversity of propagation conditions and interference and noise environments.

Several of these early detections and tracks are described in Refs. 10 through 15, which should be consulted as detailed background for this report. It should be mentioned that these two classes of radar operation have been conducted under a broad diversity of propagation path conditions. Targets have been tracked via all available ionospheric layers, from sporadic E to F<sub>2</sub>, under single-hop propagation conditions and at azimuths extending clockwise from 50 degrees through 270 degrees (true bearings from Chesapeake Beach, Maryland). However, those operations outside the azimuth interval from 050 to 110 degrees are conducted at a reduced effectiveness because the antenna which is used outside this interval suffers an approximate 14-db round-trip gain deficiency with respect to the broadside array. A limited body of experience has also been gained in tracking aircraft under two-hop propagation conditions at ranges as far as 3200 naut mi.

#### The Purpose of This Report

It is the purpose of this report to present more recent aircraft tracking data which have been obtained with the Madre research radar. In particular, the four specific characteristics of the OTH aircraft echo which have been investigated are:

- a. its utility for surveillance and tracking operations, as evidenced by time-range tracking measurements and the validity of position predictions determined from such tracks;
- b. its reliability as a radar signal, as evidenced by the extent and periodicity of amplitude scintillations during tracking observations;
- c. its utility as an indicator of target radial velocity, as evidenced by its stability in doppler shift;

d. its utility in assessing the type of target from which it is received, or in determining the number of closely spaced targets which may be discerned in it, as evidenced by its spectral distribution and the amplitude scintillations to which it is subject.

Recommendations will be made in the following text regarding some desirable parameters of a signal processing system which could be designed to fully exploit these four characteristics.

#### TIME-RANGE TRACKING OF OTH AIRCRAFT TARGETS

Prior to the spring of 1965, Madre radar data on aircraft targets were written on data sheets by the radar display observers for later reduction by manual or automatic (computer) methods. The need for a faster and more efficient method of data acquisition and reduction resulted in the development of a semiautomatic data collection system, in which paper tape is punched in a format for computer reduction.

The operation of the data collection system is the same for either real-time radar observations or postflight analysis of radar signals recorded in an analog format on magnetic tape. Thumb switches are set by the operator for the date, the radar system parameters (pulse repetition rate, frequency, azimuth, etc.), and the slant range to the leading edge of the ground backscatter. The operator periodically enters onto a keyboard a target's slant range and radial velocity as indicated by the radar display, as well as the signal strength. After these data are entered on the keyboard, the operator initiates a punch cycle in which the keyboard contents are punched on paper tape. This punch cycle requires a period of approximately 3 sec, and a trained operator is able to make a data reading and initiate a punch cycle every 10 to 20 sec.

Because of the availability of a Control Data G-15 general purpose digital computer for aircraft track analysis, the data tape is punched to be compatible with the G-15. (Punched tape in this format may readily be converted to tape suitable for reduction by NRL's larger scale NAREC computer.) Having been provided ionospheric sounding data in a separate subroutine, the computer utilizes the radar data to calculate and plot a family of ground-range vs time tracks for probable paths of propagation in the ionosphere.\*

A similar ground-range versus time track is plotted from geographical position data obtained from air-route traffic control centers, the flight navigator's logs, and/or direct radio contact with the aircraft. The radar target tracks are compared with these actual position data to evaluate the effectiveness of the Madre radar and the data reduction system in tracking aircraft under various operating conditions.

In the Class I cooperative type of operation described in the previous section of this report, preflight data is provided, and continuous radio communication between the aircraft and the Madre radar facility is possible. On May 5, 1964, one such flight was conducted with a Navy P3A Orion, the military version of the Lockheed Electra, as the target. The flight path followed by the P3A aircraft in traveling from Norfolk, Virginia, to Lajes Air Force Base, Azores, is shown in Fig. 8 with two crosshatched regions drawn to indicate those portions of the flight path in which the aircraft was tracked by the Madre radar. Radar parameters and the tracking data acquired during this P3A flight are shown in Fig. 9. In order to have ground backscatter illumination over the appropriate range interval for the planned flight path, Madre personnel selected a frequency of 15.595 Mc/s

\*This computation is described more completely in Appendix A.

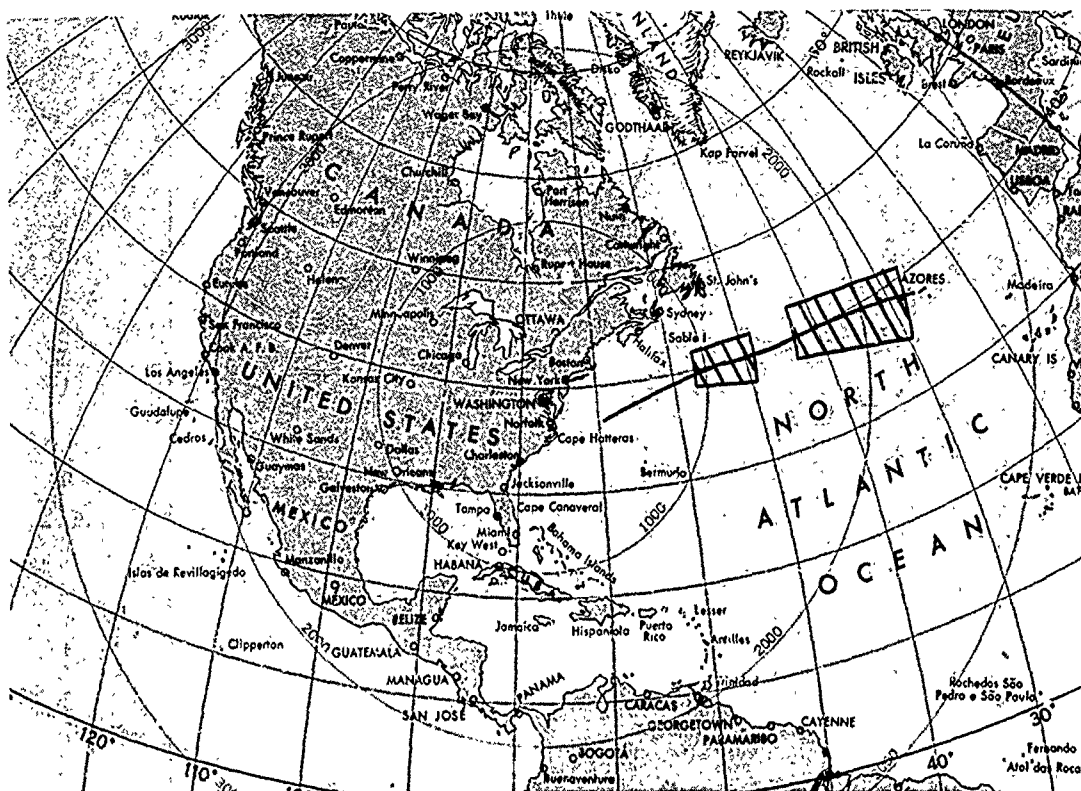


Fig. 8 - Map of radar-illuminated regions for the Class I cooperative P3A observations of May 5, 1964

(based on the National Bureau of Standards' (NBS) propagation predictions) to provide backscatter illumination from 660 to 1230 naut mi over the closer region of Fig. 8. The target was acquired at a slant range of 727 naut mi at 1151 Eastern Standard Time (EST) and, except for a 25-min interruption due to an equipment malfunction, was tracked through the illuminated area to a slant range of 1280 naut mi at 1320 EST. The operating frequency then was increased to extend the ground backscatter into the second half of the flight path. A frequency of 18.036 Mc/s provided ground backscatter from 1580 to 2640 naut mi in slant range over the farther region of Fig. 8. This frequency change required the radar to be inoperative for 25 min. The target was reacquired about 15 min after the frequency change was completed at a slant range of 1631 naut mi at 1413 EST. Tracking was interrupted 15 min later for a period of about 8 min while the prf was changed from 90 to 60 pps. The track was then continued until the target was out of the illuminated area at a slant range of 2320 naut mi at 1604 EST. The target had been tracked intermittently for 4 hr and 13 min over a ground range interval of nearly 1600 naut mi.

Both the P3A data tape punched by the radar observer and the ionospheric data obtained from the NBS ionospheric sounding station at Ft. Belvoir, Virginia, were sent to NRL's computer center for reduction by the data reduction program discussed in Appendix A. Part of the computer output was a punched paper tape used by an automatic point plotter to generate the family of ground-range vs time plots of Fig. 10. For each radar point

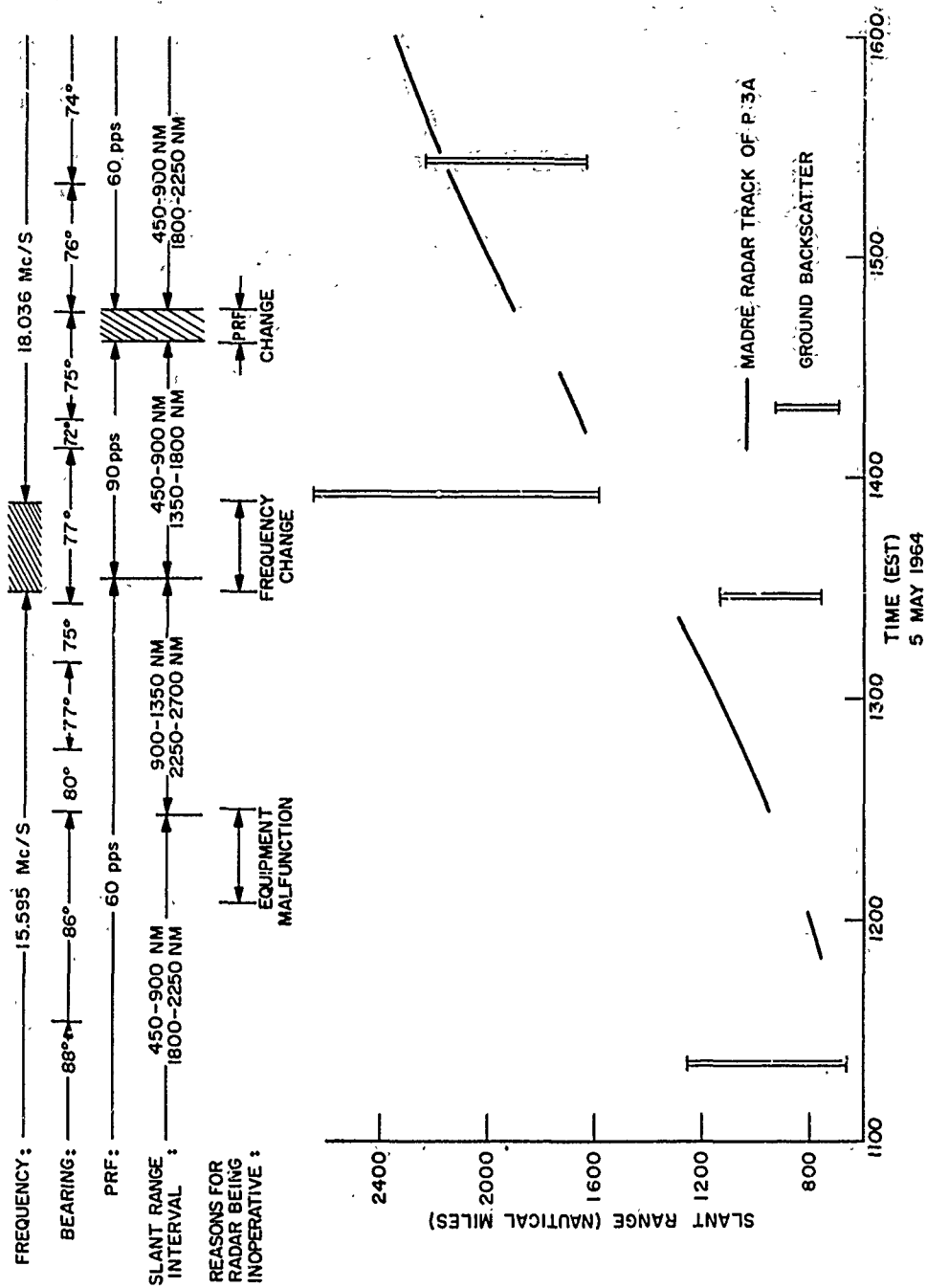


Fig. 9 - Madre radar operating parameters and tracking data acquired for the P3A aircraft flight of May 5, 1964

as many as four ground ranges, corresponding to the four possible one-hop transmission modes, were calculated and are shown in this illustration. The selection of the most probable mode must be done on the basis of available information about the different possible modes. As an aid to making this selection, the printed computer output contains such information as radiation departure angle and maximum usable frequency for all the possible modes. Often the computer itself is able to rule out an impossible mode on the basis of (geometrical) propagation parameters.\* Figure 10 shows, moreover, that even if it proves impossible to select a most probable mode by this means, the range error is nevertheless relatively small. The solid line on Fig. 10 indicates the flight path for the P3A as reported by the navigator's log. In most instances, such correspondence as is shown here between a particular mode and the actual path is readily apparent.

In the Class I noncooperative flights (in which Madre surveillance has been merely incidental to the flight), preflight data have been available to the radar operators, but very little inflight information has been acquired. An example of this type of Class I operation is the 2nd Marine Aircraft Wing's Highboy Operation: trans-Atlantic flights of F8D Crusader aircraft with refuelings from KC-130F air tankers.

The flight path of four groups of four F8D's which flew from Rota, Spain, to Bermuda on May 15, 1964, is indicated in the map of Fig. 11. One group of aircraft, Trojan Queen I, was tracked from a slant range of 1170 to 880 naut mi. In terms of ground range this track extended from 1100 to about 800 naut mi. Due to the characteristics of the ionosphere during the period of this observation, and the relatively short track involved, selection of the most probable mode of transmission is especially difficult in this case. However, through use of the methods described in Appendix B, it is possible to determine that the  $F_1$  mode of propagation was the most probable mode.

Figure 12 is a ground-range vs time plot produced by the computer from the May 15, 1964, radar data. For the sake of clarity only the points corresponding to an  $F_1$  mode have been plotted. The track produced by the inbound flight of F8D's is clearly visible. The solid line represents the reported flight path of the Trojan Queen I flight of four F8D aircraft. In addition to the high-velocity target, there appears also in Fig. 12 an intersecting low-velocity target thought to be the rescue aircraft, Duckbutt†CC. Figure 12 indicates that the track of this low-velocity target was not continuous but was, in fact, broken off at the time the high- and low-velocity target tracks appeared to intersect. It is believed that the rescue aircraft, upon intersecting the Trojan Queen I flight path, made a turn that reduced its radial velocity below the lower limit of visibility for the Madre radar's MTI processing. This explanation is somewhat substantiated by the acquisition, about 20 min later, of a similar low-velocity target at about the same range. Because no detailed position information was available, there is no solid line indicating the actual position of this target.

Very little postflight position information was available for this flight. However, the Trojan Queen I flight of four F8D's did report over Checkpoint CC, which is 1000 naut mi from the radar site, at 1008 EST. As Fig. 12 shows, this is in very good agreement with the ground-range information produced by the computer. Measured slant range to the high-velocity target at 1008 EST is 1063 naut mi. This converts to a ground range of 1004 naut mi for  $F_1$  propagation, yielding a range error of only 4 naut mi.

The main interest in tracking this flight lies in the spectrum analysis of the return signal from the Trojan Queen aircraft groups. A detailed account of this phase of the analysis appears in the next section of this report.

\*Appendix B contains a discussion of the selection process for the most probable mode.  
†Duckbutt is the tactical designation assigned to Airborne Search and Rescue aircraft.

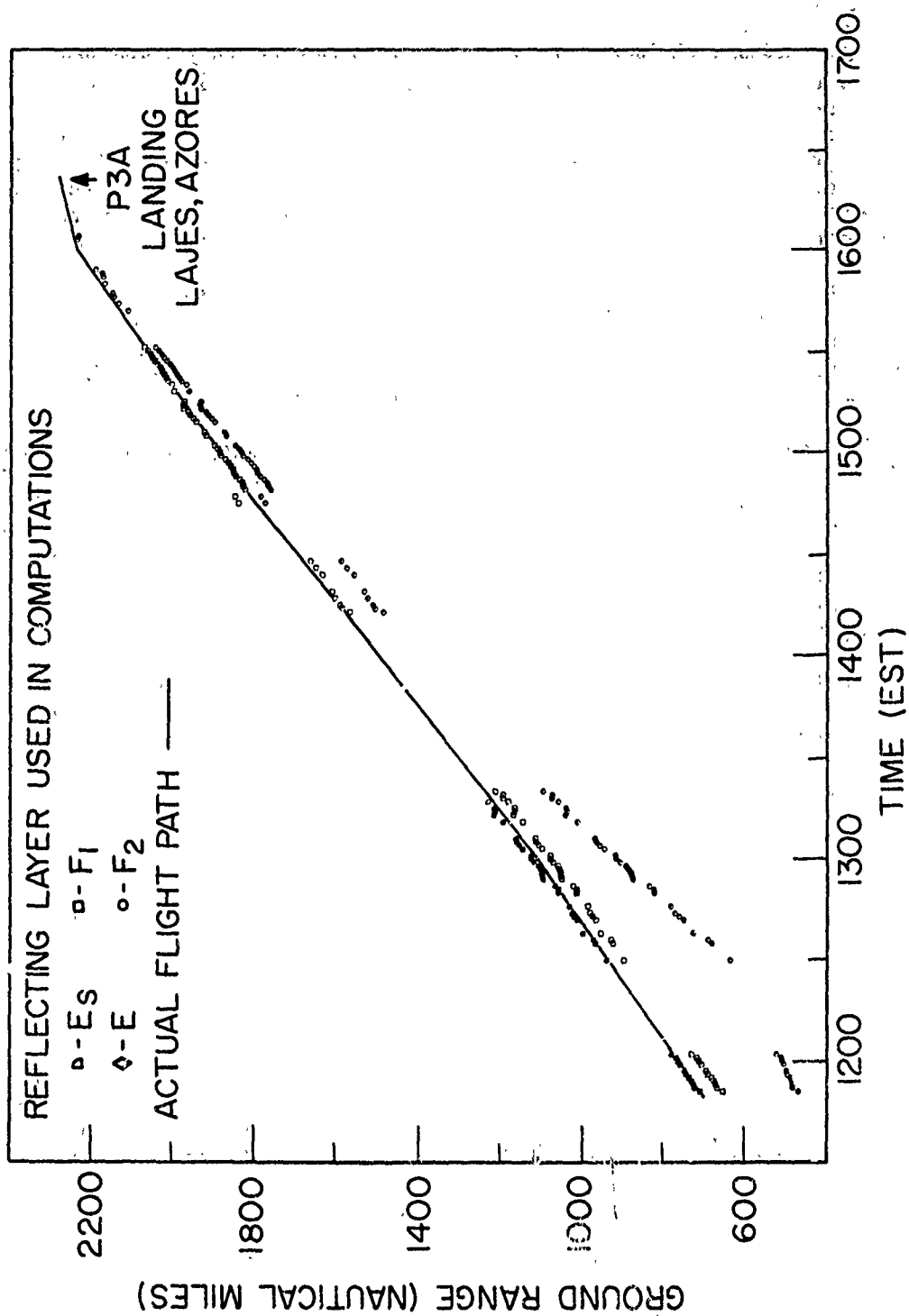


Fig. 10 - Family of ground-range vs time plots for P3A aircraft flight of May 5, 1964, as plotted from automatic data processor output. Solid line represents actual target path.



Fig. 11 - Map of illuminated region for the Class I noncooperative F8D observations of May 15, 1964

On Oct. 27, 1964, Madre surveillance operations were begun at 1400 EST at an operating frequency of 18.036 Mc/s. The broadside array was directed at a true bearing of 050 degrees in an attempt to detect aircraft targets flying the North Atlantic path, and operations continued for approximately 1 hr. Subsequent to this operating period, arrangements were made with Gander Oceanic Air Traffic Control Center to obtain flight position information (flight strips) on aircraft under Gander's control which were in the vicinity of the illuminated area. The area illuminated by the radar during this period is shown by the crosshatched area of Fig. 13. Because the antenna used during this operation has an azimuthal (two-way) 6-db beamwidth of approximately 8 degrees at this frequency, the area of adequate illumination was assumed to be 8 degrees wide.

The radar slant ranges involved were from 1200 to 2025 naut mi, as shown by the ground backscatter photograph in Fig. 14. When converted to ground ranges these limits correspond roughly to 1100 and 1950 naut mi, respectively. Because these limits placed on the illuminated area are nebulous and subject to constant change, targets outside of this area should be expected to be visible occasionally, and indeed are normally detected. This variability of the illuminated region makes the operator's problem of separating the true "within-beam" targets from the spurious "out-of-beam" targets and noise much more difficult. For example, if the operator has been tracking a target which has just faded, and at this time another target appears at roughly the correct range and velocity but is out of the main beam of the antenna, the operator may mistakenly assume this



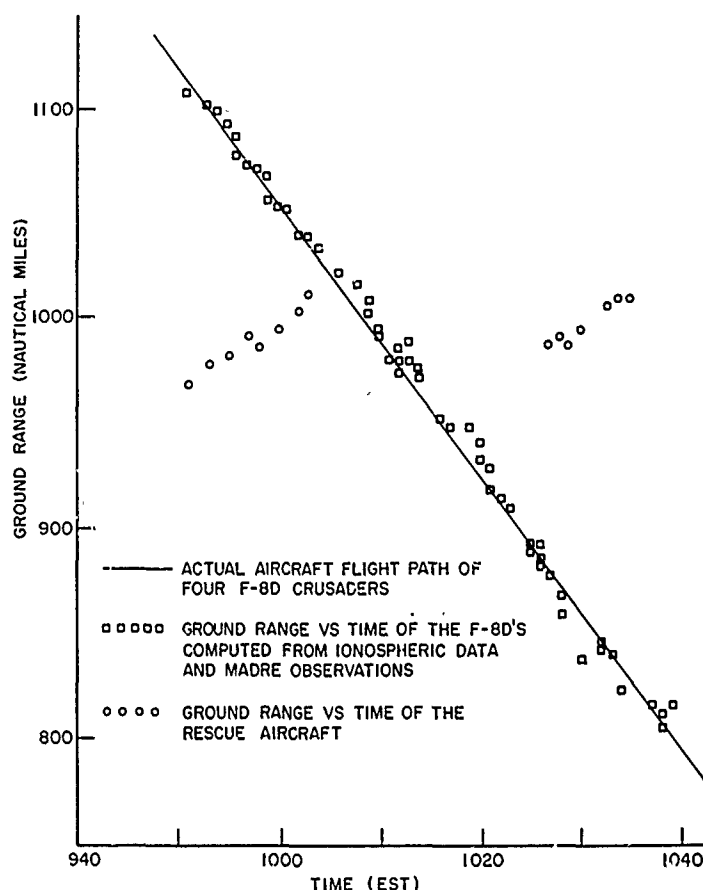


Fig. 12 - Ground-range vs time plot for the four-aircraft F8D formation of May 15, 1964, as plotted from automatic data processor output

spurious trace to be the return of his original target, and consequently, he may miss the original target when it actually returns. This situation is relieved somewhat by using a grease pencil to mark (on the face of the radar display) the positions of probable targets.

Figure 15 shows a Madre velocity vs range display of three Boeing 707's and two DC-8's which were tracked on this date and gives some indication of how the target "accounting" problem may be compounded with multiple targets.

If the raw target sightings are plotted in a slant-range vs time format, as in Fig. 16, the more persistent tracks are immediately evident. The plotting of target sightings in this manner during real-time operation would be of assistance to the radar observer in his task of separating true targets from noise and spurious signals. However, even more useful are the ground-range vs time plots generated by a digital computer from the raw slant-range vs time target sightings and data concerning the condition of the ionosphere. The method by which these computations are made for Madre observations is described in Appendix A. Such a plot, overlaid with flight strip information, is shown in Fig. 17. The computer analysis for the ionosphere during this observation period indicated that a single



Fig. 13 - Map of radar-illuminated regions for the Class I noncooperative observations of Oct. 27, 1964

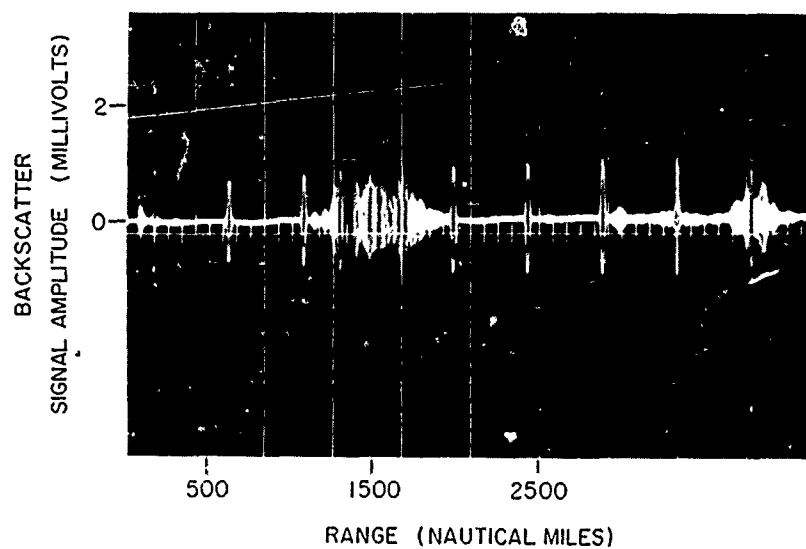


Fig. 14 - Ground-backscatter amplitude vs range format for observations of Oct. 27, 1964

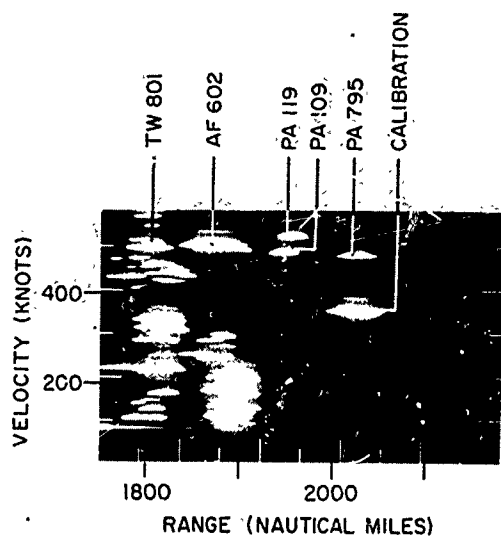


Fig. 15 - Velocity vs range display for OTH aircraft targets observed at 1417 EST on Oct. 27, 1964

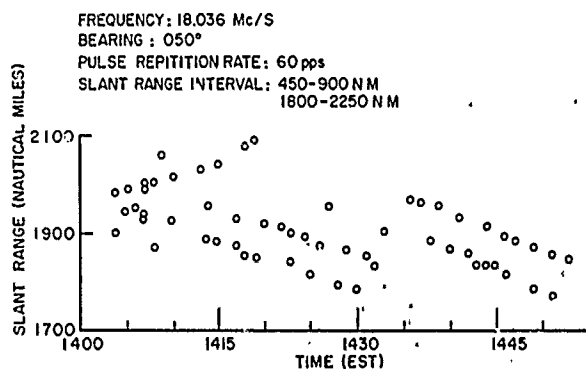


Fig. 16 - Raw slant-range vs time plots for OTH aircraft targets observed on Oct. 27, 1964

layer ( $F_2$ ) was capable of one-hop ionospheric propagation to the ranges involved, and hence the computer generated only one ground-range point for each slant-range radar point. Had other layers been applicable, as many as four points could have been generated on the ground-range plot for each slant-range point. This multiplicity of points would have complicated the analysis substantially.

Figure 17 shows that an average of about one data point per minute was taken. This data rate is normal for one operator tracking several targets simultaneously. When an operator concentrates on one target, a much denser track results, with a data rate of about two points per minute.

Considering the 8-degree azimuthal antenna beamwidth discussed above, seven aircraft flew through some portion of the illuminated area (approximately 180,000 sq naut mi in extent) during the 1-hr surveillance period of Oct. 27, 1964. All seven aircraft

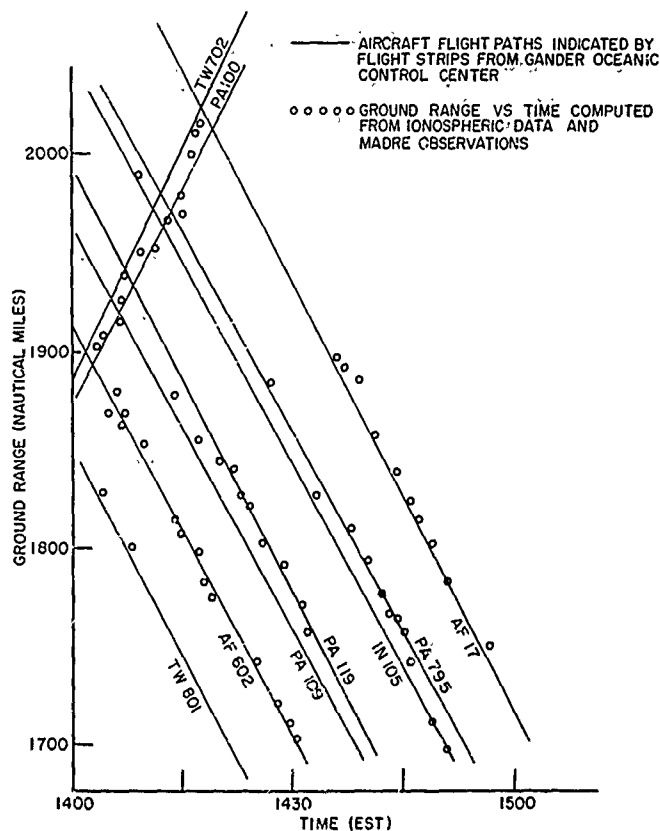


Fig. 17 - Ground-range vs time plots for OTH aircraft targets observed on Oct. 27, 1964, with overlaid flight strip information obtained from Gander Oceanic Control Center

were tracked by the radar. These targets included five Boeing 707's and two DC-8's. In addition to the seven aircraft in the 8-degree main beam, there were three more aircraft within a double beamwidth of 16 degrees. Of these three, two were tracked.

No explanation for the operators' failure to track the third "edge-of-beam" flight, LY 231 (El Al Israel Airlines, Ltd.), can be given except to say that such a low-level target may easily be overlooked while several stronger targets are being tracked. Traces and a partial track for this flight could probably be found by a close examination of photographs of the Madre velocity vs range displays.

In this blindfold radar-fence test of the Madre system, the radar detected 100 percent of the targets reported by Gander Oceanic Control Center in the normal antenna beamwidth, and 90 percent of the targets within twice the normal beamwidth (which included the above-mentioned normal beamwidth targets). No unidentified target tracks were observed. Table 3 summarizes the results of this test.

An interesting sidelight to this test was the opportunity to observe two flights with about the same radial velocity (doppler) separated in range by 30 or 40 naut mi. As may be seen from Figs. 15 and 17, three pairs of flights were of this type. During normal

Table 3  
Flights Reported by Gander Oceanic  
Air Traffic Control Within Nominal and Twice  
Nominal Antenna Beamwidths

NOMINAL BEAMWIDTH ( $\pm 1^\circ$ )			
Flight	Type Aircraft	Degrees from Beam Center	Comments*
TW 702	Boeing 707	+4	Tracked
PA 100	Boeing 707	+4	Tracked
AF 017	Boeing 707	-4	Tracked
PA 795	Boeing 707	-3	Tracked
PA 119	Boeing 707	-3	Tracked
PA 109	DC-8	-3	Tracked
AF 602	DC-8	+2	Tracked
TWICE NOMINAL BEAMWIDTH ( $\pm 8^\circ$ )			
IN 105	Boeing 720	-7	Tracked
LY 231	Boeing 707	-8	Not tracked
TW 801	Boeing 707	-8	Tracked

\*It can be seen that 100 percent of the aircraft within the nominal 8-degree beamwidth were tracked, and 90 percent of the aircraft within twice the nominal beamwidth (which includes the nominal beamwidth targets) were tracked.

tracking operations both targets of such a pair are seldom visible simultaneously, and determining that there are separate aircraft in each case is often difficult. The photograph in Fig. 15 was taken at a time when PA 119 and PA 109 were both visible. If PA 119 had not had a slightly higher radial velocity, it would have been impossible to resolve the two aircraft on the velocity vs range display. As will be shown in the next section, however, the use of a spectrum analysis technique permits very small differences in doppler to be measured, and by this means close targets may be resolved. If, however, both of the targets are not visible simultaneously, this target separation method is unreliable.

#### TEMPORAL VARIATIONS IN SIGNAL STRENGTH OF OTH AIRCRAFT RADAR ECHOES

In studying the fluctuations in echo amplitude experienced by over-the-horizon (OTH) aircraft echoes, a technique is utilized in which a doppler-range gate is oriented about a chosen target, moved in both range and doppler along with the target, and sampled periodically through a rectifier circuit to provide a record of signal amplitude versus time. In this type of analysis, samples are normally taken at a one-sample-per-second rate,

although the smoothing characteristic of the coherent signal processor stretches all large amplitude signals to at least 20 sec in length. It should be understood in considering the illustrations of signal amplitude presented below that this integration introduces an unavoidable bias toward 20-sec, and longer, periodicity in the recordings.

The coherent integration technique which permits these measurements to be made brings about an enhancement of approximately 27 db over the preintegration signal-to-noise ratio for targets whose velocities remain stable within the filter's resolution bandwidth for periods in excess of 10 sec. The values for noise level which are discussed below refer to the "effective" noise which remains, after integration, in comparison to stable-velocity targets. These noise levels are approximately 27 db below the actual preintegration radio-frequency noise with which a noncoherent radar would be confronted. The total dynamic range of the Madre signal processor for the type of measurements reported in this section is approximately 30 db. For aircraft target tracks in which echo amplitude variations in excess of 30 db have been observed, the taped echo data have been reanalyzed at different signal processor level settings. It should be emphasized, however, that the signal processor is capable of real-time operation and, in fact, that its performance in a real-time situation is somewhat superior to that possible with taped data due to synchronization difficulties associated with the tape recorder and magnetic drum speed controls on playback.

One type of operation which has been rewarding in the number and diversity of targets it has provided has been the blindfold-type operation described in the Introduction and in the previous section of this report. The brief surveillance period on Oct. 27, 1964, reported in the previous section, represents an informative example of the results which can be gained from this type operation, and five of the targets which were tracked and identified during that period have been further analyzed by the doppler-range gating technique to extract information regarding their temporal behavior. During the period of these observations, single-hop  $F_2$  layer propagation permitted illumination of targets in the range interval from about 1000 to beyond 2000 naut mi. Figure 14 is an amplitude vs range photograph of ground backscatter taken during the Oct. 27, 1964, operating period, showing also a 1-mv peak-to-peak calibration signal which appears at a 200-naut-mi range and at successive 450-naut-mi intervals. Figure 13 is a map in which the cross-hatched region indicates the area where adequate illumination was available. The observations which are discussed below were all made in the 1600- to 2050-naut-mi portion of this backscatter distribution, corresponding to the very tail of the illuminated area. Five of the aircraft targets which were tracked during this period, and which subsequently were identified, were selected for closer scrutiny with the use of the doppler-range gating technique.

Figure 18 is a conventional Madre MTI display, photographed during the Oct. 27, 1964, surveillance period, showing measured target velocity relative to the radar site along the ordinate and measured target range along the abscissa. Several targets, plus a band of noise introduced by the processing system at the extreme left, are shown in Fig. 18. Five of the strongest targets which were tracked, and which were discussed in the previous section, were chosen for more detailed analysis and these are indicated by circled numerals; the calibration signal is indicated by a circled C. This illustration represents a  $1/3$ -cps doppler-resolution display of the full available doppler extent of 30 cps, or 485 knots. The five targets identified in Fig. 18 will be referred to below by the designations assigned to them by aviation control centers from whose data the radar targets were identified. These designations are indicated in Table 4, together with the circled numerals which appear in Fig. 18. It should be noticed in Table 4 that targets 1 and 3 are denoted as compound targets. The aircraft which compose these targets were quite close together in both radar range and in doppler, or velocity, and the radar data which appears below

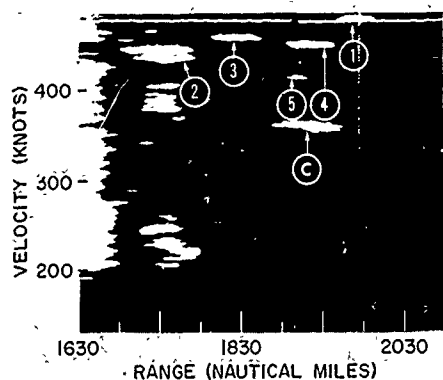


Fig. 18 - Velocity vs range display for OTH aircraft targets observed at 1419 EST on Oct. 27, 1964.(compare with Fig. 15)

Table 4  
Five Aircraft Targets Tracked by the  
Madre Radar on Oct. 27, 1964

Target No.	Control No.	Type of Aircraft	Operator
1 (compound)	PA 100 TW 702	Boeing 707 Boeing 707	Pan American Airlines Trans-World Airlines
2	AF 602	DC-8	Air France
3 (compound)	PA 119 PA 109	Boeing 707 DC-8	Pan American Airlines Pan American Airlines
4	PA 795	Boeing 707	Pan American Airlines
5	IN 105	Boeing 720	Aerlinite Eireann

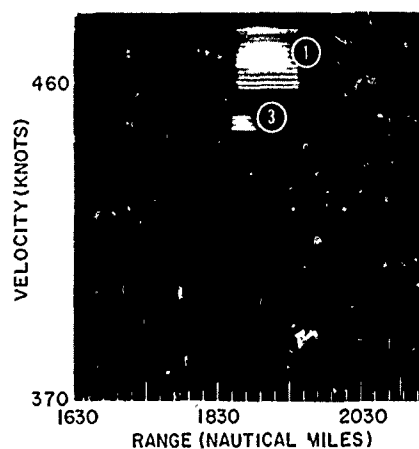


Fig.19 - Expanded display of velocity vs range for OTH aircraft targets observed at 1405 EST on Oct. 27, 1964

for these two targets contain unresolved information from the two aircraft listed in each case. No attempt was made to separate the individual aircraft in each case, although the spectral characteristics of such multiple-aircraft targets permit them to be separated. This circumstance is treated in detail in the next section of this report.

Figure 19 is an expanded-scale display of velocity vs range showing two of the numbered targets in a 6.8-cps (110-knot) portion of the doppler spectrum. The upper target is enclosed in a 1-cps  $\times$  100-naut-mi doppler-range gate whose output contains the information which is recorded on chart paper to provide continuous signal amplitude information.

Figure 20(a) shows a pair of chart paper recordings of the signal amplitude, or apparent radar cross section, data which were obtained for the compound target PA100/TW702, the only receding target of the five selected for analysis. Along the bottom of each chart is a time scale (EST), and measured values of ground range at selected intervals along the track are also included. Scales of signal amplitude or apparent radar cross section appear on the left-hand side of the records; a brief explanation of the latter scale is in order.

The values shown for apparent radar cross section were calculated from the corresponding signal amplitude values which appear on Fig. 20 and represent a very rough estimate of this parameter. In computing these values, a single value for radar range, selected to be the target range at the center of the observed interval, was utilized. A slight error thus exists for data at the extremes of the chart. Secondly, in computing the radar cross-section figures, the signals were (rather artificially) presumed to be received at the peak of an antenna lobe, and hence the peak effective gain of the antenna was utilized in making the calculation. This procedure for estimating antenna gain tends to make all apparent radar cross-section values underestimates of the true values. Finally, in order to approximate ionospheric losses, a constant loss value of 12 db, in addition to spreading loss, was included in the calculation. These circumstances apply as well to similar data for other targets to be discussed subsequently.

The lower chart in Fig. 20(a) contains information which was analyzed at a high signal processor level, permitting the lowest amplitude portion of the aircraft echo signal to be recorded at the expense of a slight limiting in the highest amplitude portions. The integrated or "narrow-banded" noise level in Fig. 20(a) is approximately 0.1  $\mu$ v peak-to-peak (p-p), and the threshold is adjusted so that this "effective" noise just appears on the record. It should be borne in mind that this noise is approximately 27 db below the pre-integration noise level. The upper chart contains the same information as the lower chart, except that the signal processor was adjusted to avoid saturation of the highest amplitude portions of the signal, and the threshold had to be set slightly above the effective noise level in keeping with the 30-db dynamic range of the signal processor. A principle feature of Fig. 20(a) is that the signal undergoes distinct fading, with peak-to-null ratios of 20 to 30 db. The unavoidable bias in the Madre signal processor to periodicities of 20 sec and longer should be apparent as well. The data in Fig. 20(a) represents a target which recedes out onto the tail of the backscatter distribution and displays a gradually decreasing character both in gross signal amplitude and in fading depth as the illumination decreased.

Figure 20(b) contains similar data for a second target (AF 602) which approached through an adjacent range interval during the same period. Once again, two signal processor levels are represented by the two charts, although the highest amplitude portions of Fig. 20(b) are markedly higher than those in Fig. 20(a). This circumstance is explained by the fact that AF 602 was in a region of higher ground backscatter (and thus was more intensely illuminated) and was also closer to beam center than PA100/TW702.



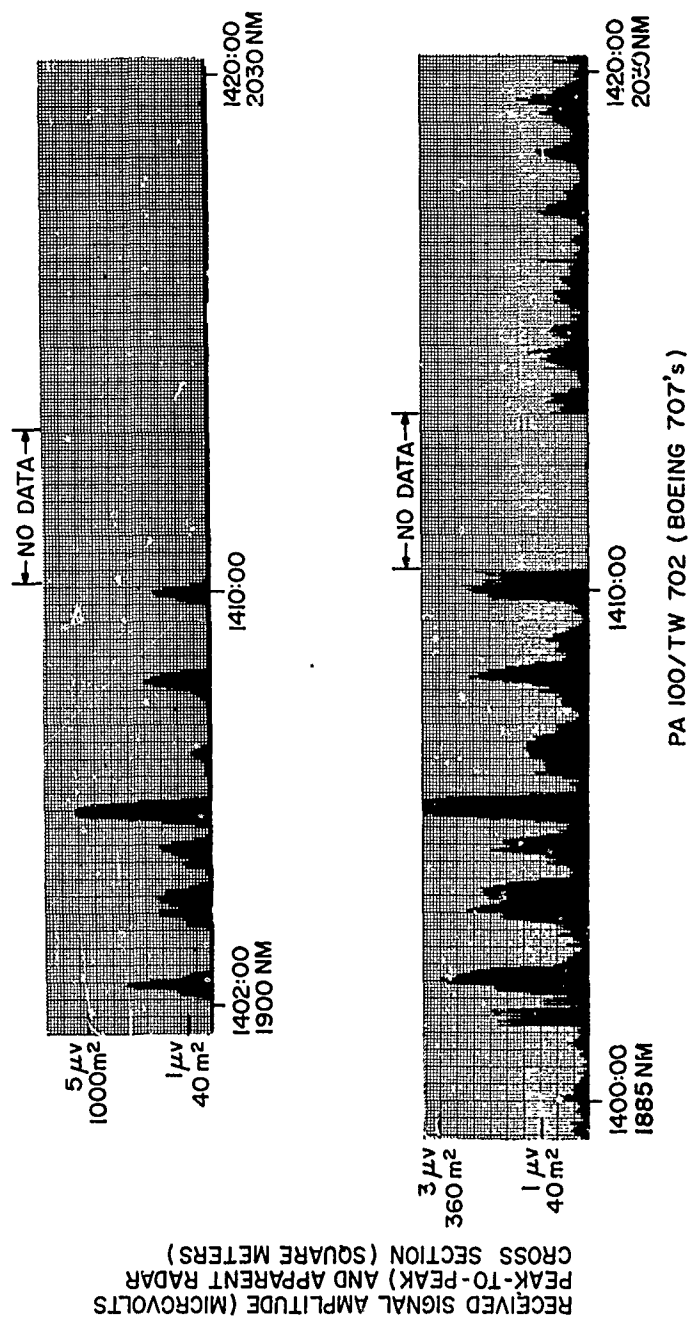
The lower chart contains the data made with a high signal processor level and shows the integrated noise at approximately  $0.1 \mu\text{v p-p}$ . Once again, fading with a periodicity of 20 sec and longer is evident, and fading null depths of approximately 30 db and deeper are frequent. The upper chart contains data for the low signal processor level and displays the highest amplitude portions of the record.

Figure 20(c) contains further apparent radar cross-section data for another approaching target (PA119/PA109) which passed through the 1600- to 1900-naut-mi range interval during a somewhat later period. As above, two signal processor levels are represented in Fig. 20(c), permitting the lowest amplitude portions and the highest amplitude portions of the track to be displayed. The integrated noise level for this record is approximately  $0.1 \mu\text{v p-p}$  averaged across the record, and once again, the 30-db fading depths and the 20-sec, and longer, periodicity may be readily discerned. A longer time scale periodicity is also evident in Fig. 20(c), displaying peaks at approximately 1420 and 1440 EST. Similar 15- to 30-min periodicities have been observed during other aircraft observations, and also in connection with lunar radar experiments which have been conducted with the same apparatus (16). The lunar echo's fading pattern has normally been separable into recognizable components attributed to polarization-rotation associated with the ionospheric Faraday effect, and to the variation of the antenna pattern in elevation; neither of these phenomena has explained the 15- to 30-min periodicity similar to that displayed in Fig. 20(c). It is believed that a likely source of this periodicity is the passage of ionospheric irregularities through the propagation path. Tveten (17-18) has reported that traveling ionospheric anomalies often display apparent periodicities of this time scale, and such disturbances could cause focusing effects which would give rise to the peaked behavior displayed at 1420 and 1440 EST in Fig. 20(c). Other examples of this behavior appear below.

The shorter time scale periodicity, varying in period from less than 20 sec to more than a minute, is a normal characteristic of OTH radar echoes. It is this fading which may be attributed in part to a polarization fading effect, although a second and possibly stronger contribution is believed to be an interference-type fading due to the existence of a multiplicity of paths. This belief is reinforced by (a) the fact that the short time scale periodicity is distinctly more pronounced during periods in which a target is passing through a peak of the backscatter distribution than when it is passing through a region in the tail of the backscatter, and also by (b) some differences between the single aircraft echo behavior displayed in these illustrations and multiple aircraft echo behavior, which is treated below.

Figure 20(d) contains yet another pair of signal amplitude, or apparent radar cross-section, charts for PA Flight 795 approaching through the same range interval. The familiar 20-sec, and longer, fading behavior and 30-db fading null depths are present in Fig. 20(d) once more, and the integrated noise level is  $0.1 \mu\text{v p-p}$  as previously. One feature which is worthy of note in Fig. 20(d) is the single, extremely strong peak at approximately 1425 EST. This peak may confidently be said to result from an extreme focusing situation and is an example of an echo which could easily be discerned without the coherent MTI signal processing which is necessary most of the time. It is this type of echo which a noncoherent radar can detect if it possesses adequate power and antenna gain characteristics.

Figure 20(e) shows a pair of signal amplitude, or apparent radar cross-section, charts for another approaching target (IN 105) tracked during the Oct. 27, 1964, observation period. The 30-db fading structure and the 20-sec to 1-min periodicity are present again in Fig. 20(e); the integrated noise level is approximately  $0.1 \mu\text{v p-p}$  once more.



(a)

Fig. 20 - Signal amplitude, or apparent radar cross section, vs time (EST) and range for (a) compound target Pan American Airlines Flight 100 and Trans-World Airlines Flight 702, measured on Oct. 27, 1964

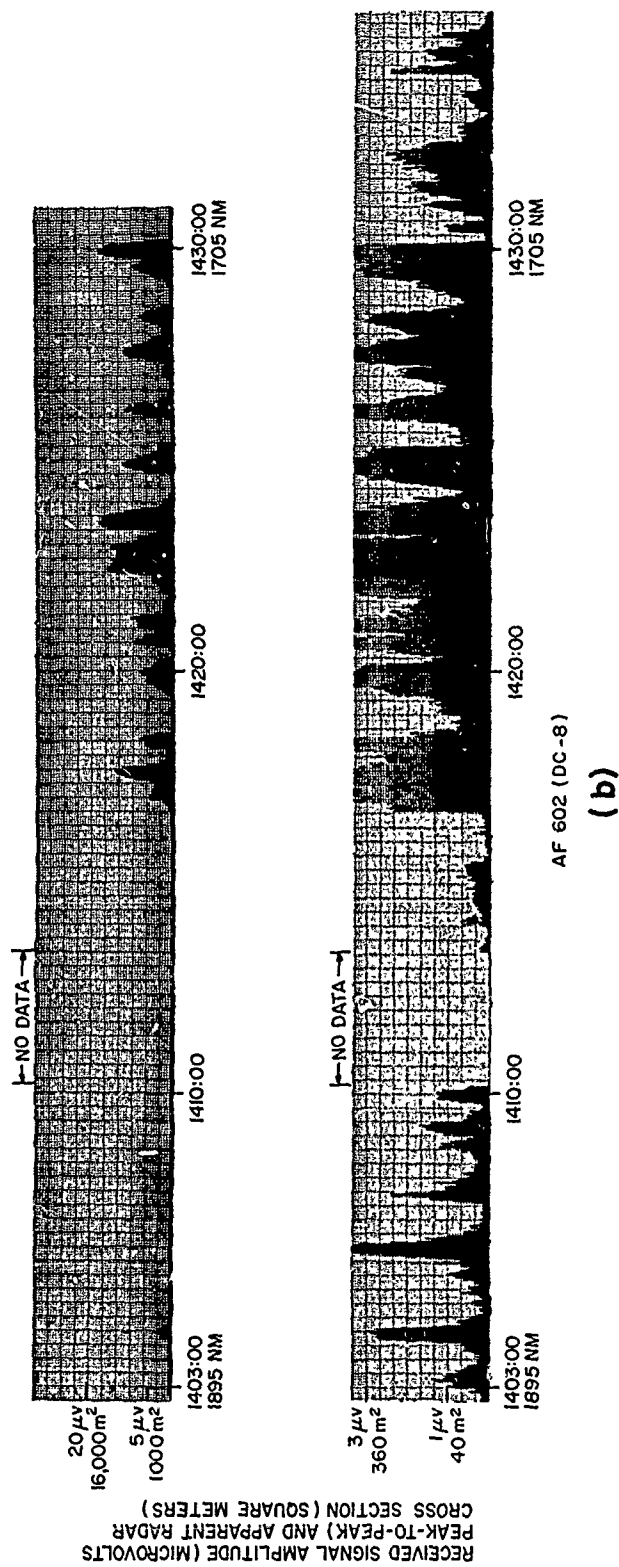


Fig. 20 (cont'd.) - Signal amplitude, or apparent radar cross section, vs time (EST) and range for  
(b) Air France Flight 602, measured on Oct. 27, 1964

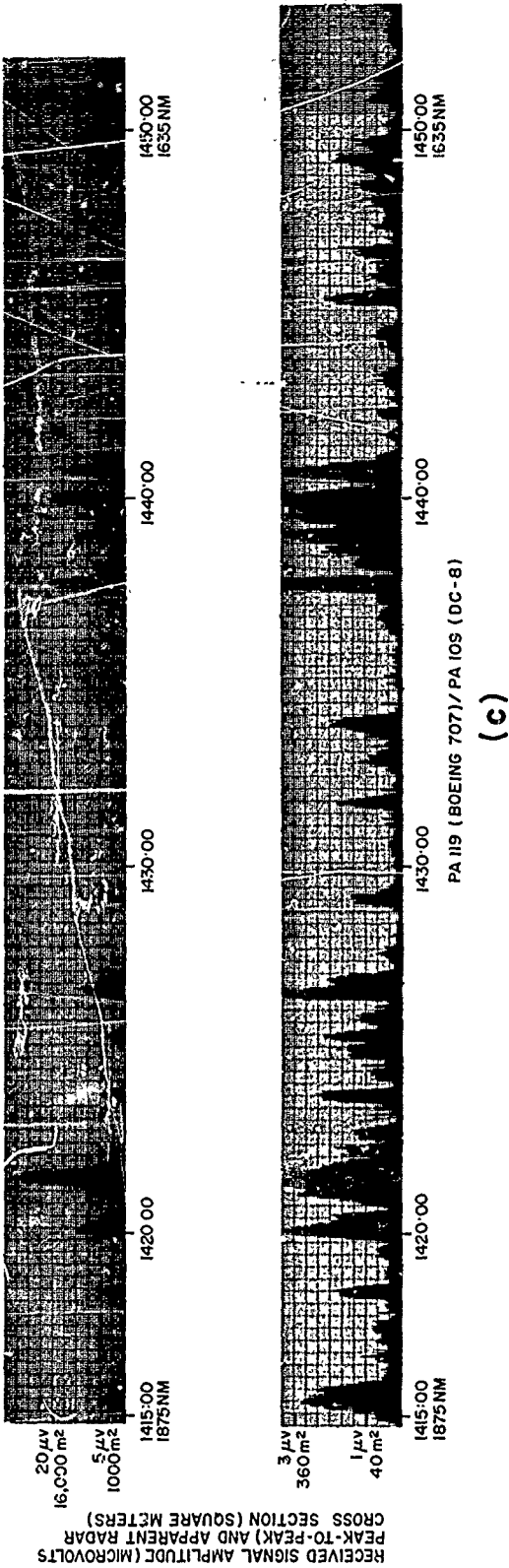


Fig. 20 (cont'd.) - Signal amplitude, or apparent radar cross section, vs time (EST) and range for (c) compound target, Pan American Airlines Flights 119 and 109, measured on Oct. 27, 1964

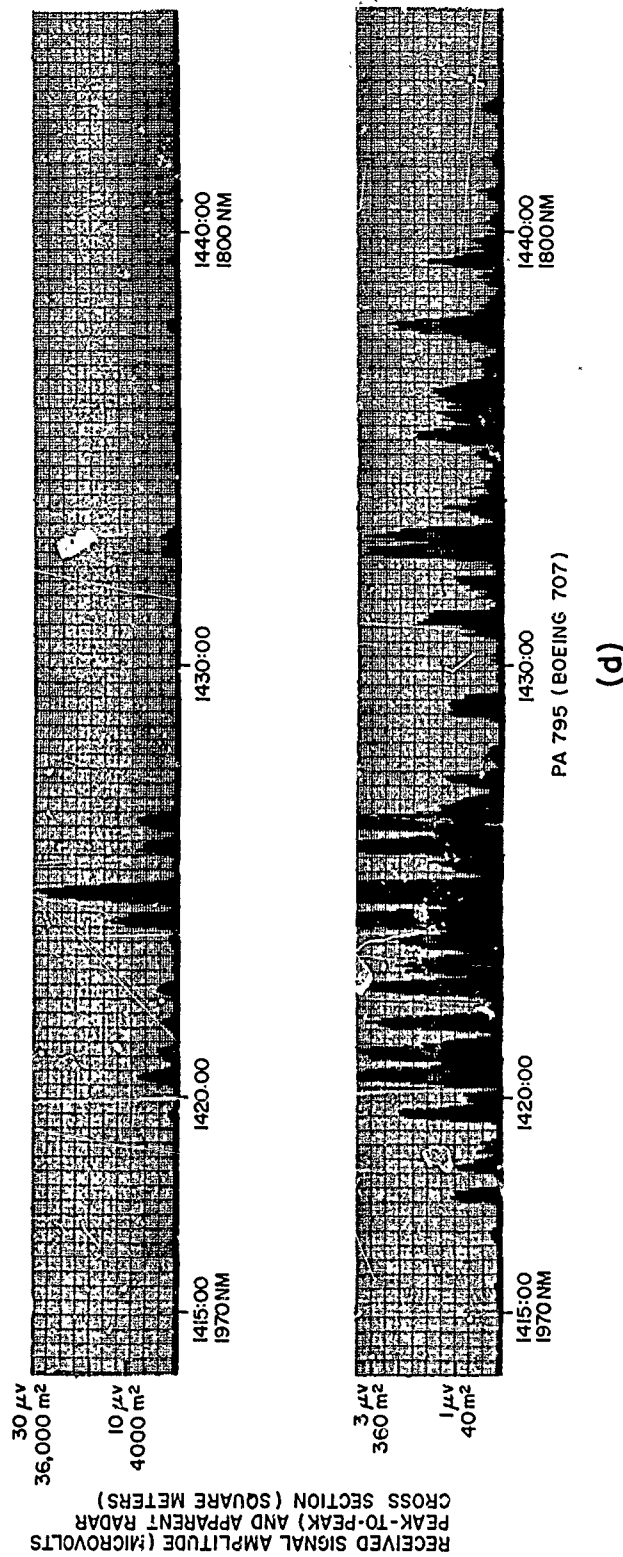


Fig. 20 (cont'd.) - Signal amplitude, or apparent radar cross section, vs time (EST) and range for  
(d) Pan American Airlines Flight 795, measured on Oct. 27, 1964

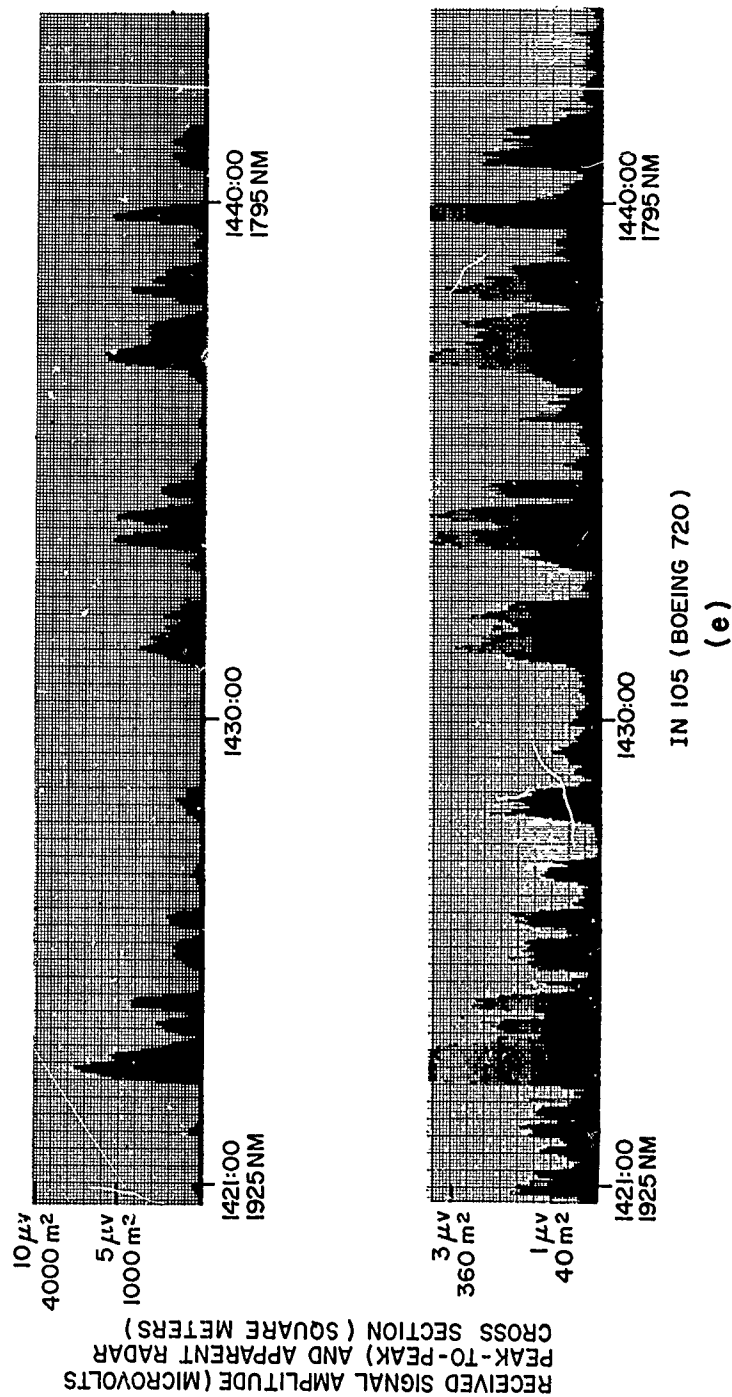


Fig. 20 (cont'd.) - Signal amplitude, or apparent radar cross section, vs time (EST) and range for  
(e) Airlinte Eireann Flight 105, measured on Oct. 27, 1964

The information contained in Figs. 20(a) to (e) is amenable to a simple form of statistical analysis, and it is believed that a brief treatment of its significance can be based on a rudimentary discussion of the likely detectability of an OTH aircraft target under various system sensitivity conditions. It is believed that the 27-db signal-to-noise enhancement provided by the Madre signal processor represents a practical optimum in view of the doppler stability of the OTH aircraft target and the likely scanning requirements for a surveillance radar. It also is believed that the power and antenna gain characteristics of the Madre system represent, at least, a reasonable estimate of the likely parameters for such a radar, and hence these characteristics are treated below as the basis for this detectability analysis.

A somewhat arbitrary constraint on a target signal is imposed in order that a target may be acquired on a single scan of the Madre analysis filter, that is, on a single complete display of the integrated radar data; the signal must possess a signal-to-integrated-noise ratio of at least 10 db at the signal processor output. This constraint is no doubt a rather artificial one, but it permits a simple and, hopefully, illustrative picture to be drawn of the implications of these data. Table 5 contains a listing of several parameters calculated from Figs. 20(a) to (e). The first column in Table 5 is a list identifying the five aircraft targets. The second column is a list of the mean apparent radar cross section for the five targets, scaled from the apparent radar cross-section charts with the aid of a planimeter. The third column is a list of mean integrated signal-to-noise ratio values computed from (a) the apparent radar cross-section data and (b) the measured integrated noise values for the five tracks. The fourth, fifth, and sixth columns contain, respectively, the mean percentage of the time, during each of the five tracks, when the signal amplitude exceeded a level of 10, 20, and 30 db above the integrated noise. The seventh, eighth, and ninth columns contain, respectively, the mean time between the successive occurrence of detectable echoes at these same levels of 10, 20, and 30 db above the integrated noise level. No figures have been computed in columns 7 and 9 for those cases in which acquisition on a 10-db signal-to-noise ratio could be made more than 50 percent of the time.

Table 5  
Statistical Behavior of OTH Aircraft Echoes Recorded on Oct. 27, 1964

Target	Mean Apparent Radar Cross Section ( $m^2$ )	Mean Integrated S/N Ratio (db)	Percent of Time That Integrated S/N Greater Than:			Mean Time Between Successive Peaks for Which S/N Greater Than:		
			10 db	20 db	30 db	10 db	20 db	30 db
PA 100/TW 702	6	12	60%	32%	1.5%	-	65 sec	600 sec
AF 602	230	27	81	59	15	-	-	90
PA 119/PA 109	116	24	55	26	4	-	73	316
PA 795	110	24	41	28	5	38 sec	58	220
IN 105	53	21	63	43	7	-	40	208

Despite the limited number of observations presented in Table 5, the table represents a typical distribution of target behavior. Targets IN 105 and PA 100/TW 702 are aircraft which were tracked either through regions at the edges of the antenna beam or through a lower portion of the backscatter distribution than were the other three targets. Their behavior is illustrative of small targets. The other targets all behave in a manner similar to most targets at ranges of 1800 naut mi under favorable propagation conditions, displaying mean, apparent, radar cross sections of 100 to 200  $m^2$ . These values of 100-200  $m^2$  represent the apparent radar cross sections and should not be confused with radar cross sections which would be measured on a line-of-sight basis. Such matters as polarization alignment have not been considered in these measurements, and propagation losses have been estimated only roughly.

SECRET

It should be evident from Table 5 that under the constraint specified above as a condition for single-look acquisition of a target, namely, that its signal-to-integrated-noise ratio should exceed 10 db, typical OTH aircraft targets should be visible, on an average, about 60 percent of the time. It should also be evident that a noncoherent radar, which would probably suffer at least a 20-db deficiency in signal-to-integrated-noise ratio when compared to a Madre-like system, would be able to acquire these targets only about 6 percent of the time and, hence, would have to remain on each range-azimuth coverage interval substantially longer. The ninth column in Table 5 indicates that a noncoherent radar would be required to remain on a single coverage interval for an average of nearly 5 min in order to detect all targets, while a coherent, Madre-type radar would need to remain for only a few seconds, perhaps two 10-sec integration periods separated by a few minutes. This comparison of a noncoherent radar with a Madre-like system is, however, incomplete in that it neglects the serious problem of subclutter visibility to which the former is subject. It is assumed in making the comparison that some means is available to the noncoherent radar to achieve subclutter visibility in the range from -50 to -100 db signal-to-clutter ratio. But no such means has been disclosed to the present authors as yet.

The Class I cooperative P3A flight of May 5, 1964, furnishes an illustration of the degree to which an OTH radar may be used for tracking selected targets over extended range intervals. During the May 5, 1964, observation period, a U.S. Navy P3A aircraft was tracked over a range interval extending from 725 to 2320 naut mi, with a brief interruption of coverage in midcourse due to a radar malfunction. The behavior of the aircraft echo received over the widely varying propagation paths which were required for illumination over this extended range interval has been studied in some detail. Figure 8 is a sketch of the flight path followed by the P3A aircraft in traveling from Norfolk, Virginia, to Lajes AFB, Azores, with two crosshatched regions drawn to indicate the areas through which the aircraft was tracked.

The closer region, extending from 900 to 1300 naut mi in range from the Madre installation, corresponds to an area in which the aircraft's passage through the tail of an  $F_1$ -layer backscatter distribution has been studied. The remote region, extending from 1600 to 2250 naut mi in range, corresponds to an area in which the target's passage through the peak and down into the tail of an  $F_2$ -layer backscatter distribution has been studied. The widths of the two crosshatched regions give an indication of the 3-db (one-way) azimuthal beamwidths of the broadside array at the frequencies utilized for illumination of this P3A aircraft.

Figure 21(a) is a chart of signal amplitude, or apparent radar cross section, for the P3A aircraft during its passage through the closer illumination interval. The apparent radar cross-section values indicated with the corresponding signal amplitude labels in Fig. 21(a) have been determined by the same means described above and should be regarded simply as rough estimates. The integrated noise level in Fig. 21(a) is approximately 0.2  $\mu$ v p-p, as indicated by the lowest amplitude portions of the chart. It should be noted in Fig. 21(a) that the signal never exceeds a level of approximately 3  $\mu$ v p-p or 53 m<sup>2</sup> apparent radar cross section, corresponding to a maximum signal-to-effective-noise level of approximately 20 db. The rather low peak amplitude and 20-db signal dynamic range displayed in Fig. 21(a) has been found to be typical of OTH aircraft echoes from targets which are well displaced beyond the actual peak region of the ground backscatter distribution. The familiar 20-sec, and longer, peak duration and a peak separation of several minutes is evident in Fig. 21(a).

Figure 21(b) contains similar data for the later portion of the P3A flight, in which the aircraft was passing through the 1600- to 2250-naut-mi range interval. Figure 21(b)



was made at a similar signal processor level for comparison with Fig. 21(a), but due to the fact that the aircraft in Fig. 21(b) was at nearly twice the distance as when Fig. 21(a) was made, the corresponding apparent radar cross-section values are more than an order of magnitude higher in Fig. 21(b). It should be noted also in Fig. 21(b) that the signal frequently exceeds the  $3 \mu\text{V}$  p-p level, which was found in Fig. 21(a) to be a maximum, and, in fact, saturation of the processing and recording equipment is evident during nearly one-fifth of the track in this illustration. This behavior is attributed to the circumstance that during the later period the aircraft was passing through the peak of an  $F_2$ -layer backscatter distribution, in which a substantial degree of energy focusing was believed to exist. Notice in Fig. 21(b) that the echo does periodically drop into the integrated noise at approximately  $0.10 \mu\text{V}$  p-p and spends several minutes between 1515 and 1520 EST below a detectable level. The period between 1530 and 1540 is representative of noisy, but usable data. During this period an interfering station caused considerable degradation of the signal amplitude data, but a readable signal was present most of the period. Previously acquired targets can often be tracked through such interference, but not usually without some difficulty. Figure 21(c) contains the same data as Fig. 21(b), but in this case the signal processor level has been adjusted to avoid saturation at signal amplitude peaks. Several signal peaks in the 20- to  $30\text{-}\mu\text{V}$  p-p range are evident in Fig. 21(c). The total dynamic range of the signal in the later portion of the P3A track extends from the  $0.1\text{-}\mu\text{V}$  p-p effective or integrated noise level to more than  $30 \mu\text{V}$ , a range in excess of 40 db. This extreme range of signal fluctuation has been found to be the rule for aircraft targets tracked through the peak of a backscatter distribution during favorable propagation conditions. Once again, in Fig. 21(c) a long time scale periodicity is evident. Despite the pronounced regularity of this fading, it cannot be readily correlated with antenna lobe structure. The credibility of attributing even this strikingly regular behavior to ionospheric irregularities is increased when it is understood that its appearance is extremely sporadic and seldom obeys so regular a pattern of fading.

Table 6 contains pertinent statistics for the two periods of observation of the P3A aircraft and emphasizes the striking contrast between the behavior of an aircraft in a backscatter distribution peak and the behavior of one well displaced from the peak toward the tail of that backscatter distribution. A target which can be considered "acquirable" only 25 percent of the time under the latter conditions can be seen almost at will under the former circumstances.

The fortunate circumstance that the P3A aircraft was observed during a period in which it passed through the peak and into the tail of a ground backscatter distribution permits an illustrative discussion of signal-to-clutter ratio to be presented. Figure 22 is a photograph of the amplitude vs range distribution of ground clutter which was taken during the later portion of the P3A observation. The white line drawn through the peak of the clutter distribution and down along the tail of the contour represents an approximated distribution which was used for the purpose of calculating rough signal-to-clutter ratios during this period. Figure 23 is a plot of calculated signal-to-clutter ratios taken from the signal amplitude data in Figs. 21(b) and (c), utilizing the approximated clutter contour in Fig. 22. Individual vertical lines in Fig. 23 correspond to samples of target signal taken at 20-sec intervals. The system threshold is seen to be initially at a signal-to-clutter ratio of approximately -100 db, corresponding to the level at which residual clutter penetrates the Madre comb-rejection filters. This condition exists for this observation only during the period in which the target remains within the very peak of the backscatter. As the target passes into the tail of the distribution and other types of noise become dominant over residual clutter, the system threshold is seen to rise gradually. It should be evident from Fig. 23 that signal-to-clutter ratios of from -100 db to -50 db are of concern throughout the observation period. This range of signal-to-clutter variation has been found to be the rule for OTH aircraft tracking. In fact, the effects of rather

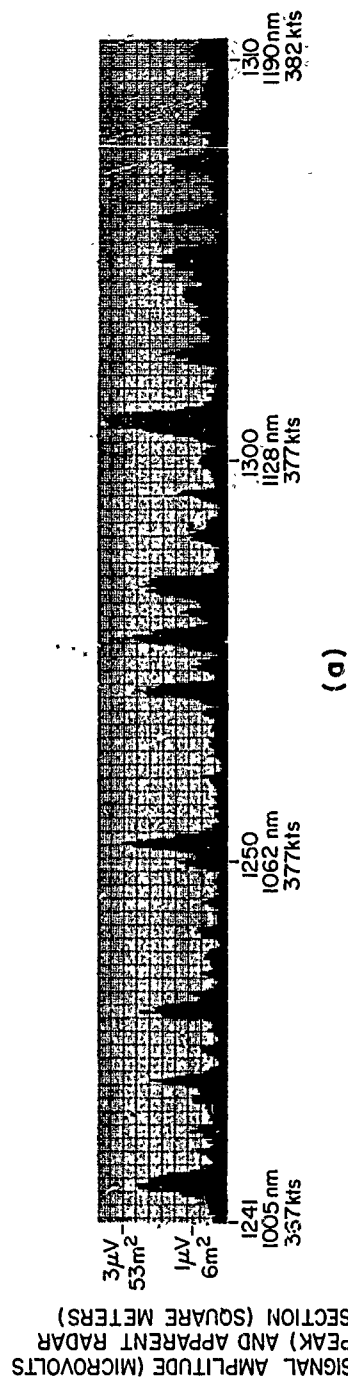


Fig. 21 - Signal amplitude, or apparent radar cross section, vs time (EST), range, and velocity for  
(a) early portion of P3A aircraft track, for May 5, 1964 observation

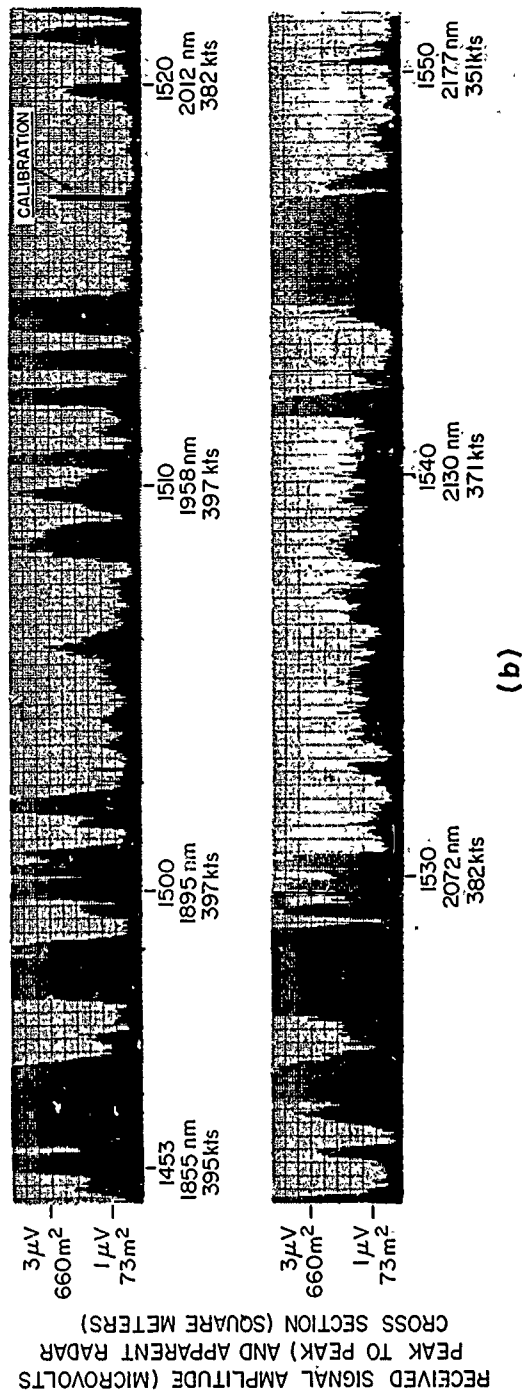


Fig. 21 (cont'd) - Signal amplitude, or apparent radar cross section, vs time (EST), range, and velocity for  
(b) later portion of P3A aircraft track, with high processor level, for May 5, 1964 observation

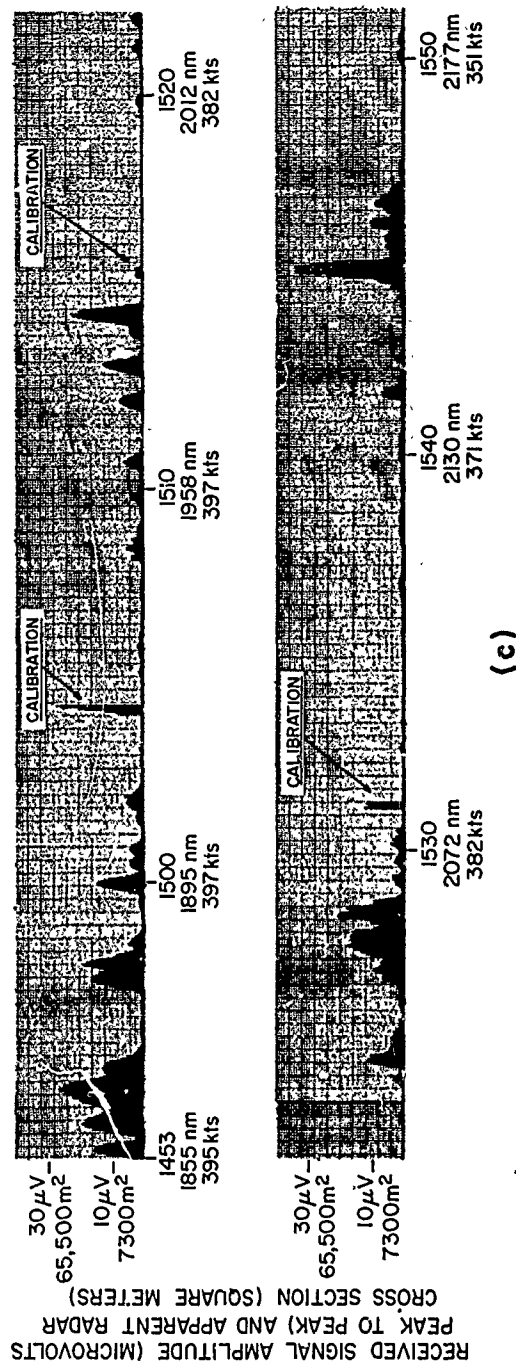


Fig. 21. (cont'd) - Signal amplitude, or apparent radar cross section, vs time (EST), range and velocity for (c) later portion of P3A aircraft track, with low processor level, for May 5, 1964 observation

Table 6  
Statistical Behavior of OTH P3A Aircraft Echoes  
Recorded on May 5, 1964

Range Interval (naut mi)	Mean Radar Cross Section ( $m^2$ )	Mean S/N Ratio (db)	Percent of Time That S/N Greater Than:			Mean Time Between Successive Peaks for Which S/N Greater Than:		
			10 db	20 db	30 db	10 db	20 db	30 db
900-1100	3.4	11	25.4%	9.6%	0%	58 sec	142 sec	-
1600-2250	700	26	-	50	17	-	50	164 sec

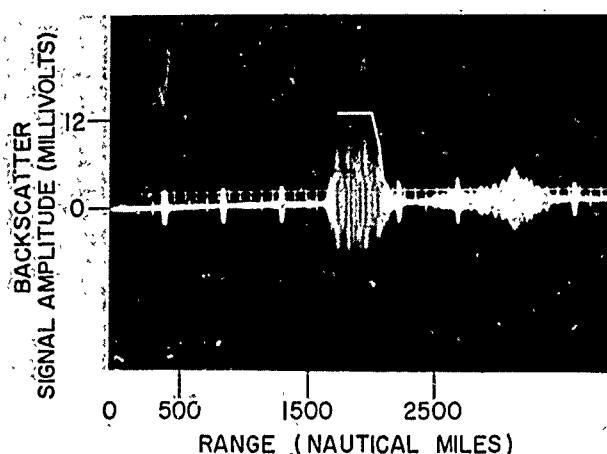


Fig. 22 - Ground backscatter amplitude versus range format for observations of May 5, 1964

extreme energy focusing, which give rise in this case to apparent radar cross-section values approaching  $10^5 m^2$ , cannot be seen to reduce the need for clutter-rejection filtering. Indeed, it can be seen from Fig. 23 that even additional clutter filtering might have been useful during periods such as those around 1505 EST and between 1515 and 1520 EST.

The flights of group formations of Marine Corps F8D interceptor aircraft on May 15, 1964, treated in the previous section of this report from a tracking standpoint, represented a valuable opportunity for the study of multiple-aircraft echoes, that is, of echoes from a closely spaced group of targets within the range-resolution limit of the Madre radar. During the flights of two groups of these aircraft from Rota, Spain, to Beaufort, N.C., observations were conducted in a region extending from 700 to 1200 naut mi east of the Madre installation, as indicated by the crosshatched region in Fig. 11. A series of observations was also conducted at the same time of tanker and rescue aircraft associated with the F8D crossing, flying within the same interval. All observations were made via  $F_1$ -layer propagation.

Figure 24(a) is a pair of signal amplitude, or apparent radar cross-section, charts recorded at different signal processor levels for overlapping portions of a period in which a group of four F8D aircraft was tracked from approximately 1100 naut mi in to

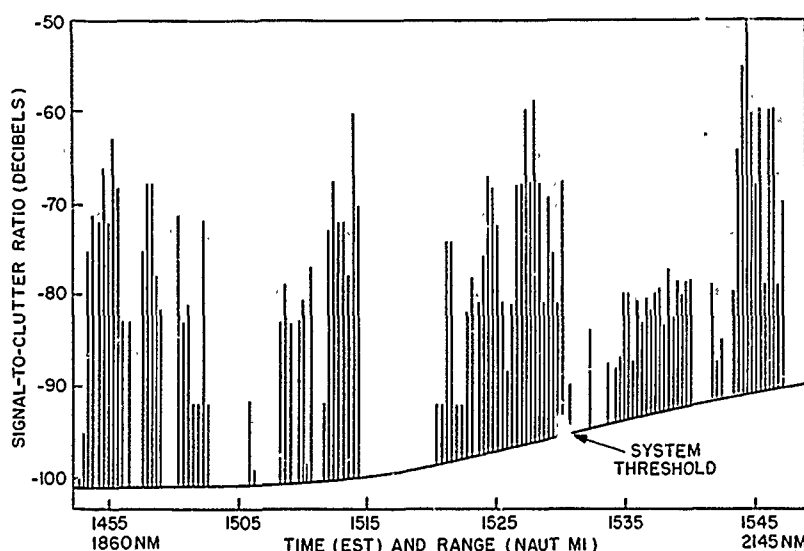


Fig. 23 - Calculated signal-to-clutter ratios for P3A aircraft track of May 5, 1964

800 naut mi in range. The upper chart was recorded at a rather high signal processor level to provide a display of the very lowest amplitude portions of the track. The integrated noise level in Fig. 24(a) is approximately  $0.1 \mu\text{v}$  p-p, a level to which the multiple-aircraft echo amplitude may be seen to descend very rarely. The single most striking feature of this multiple-aircraft track, which sets it apart from all single-aircraft tracks, is the fact that its fading structure displays a distinct tendency to remain free of deep nulls below the integrated noise level.

During the interval included in the upper chart of Fig. 24(a) the four-aircraft formation approached through the tail toward the steeply rising portion of the ground-backscatter contour. The dynamic range of the signal was restricted to a 20-db interval during this period, as is typical of OTH aircraft echoes in the tail of the backscatter. As the formation grew close to the steeply rising peak of the distribution, both the maximum-amplitude portions of the record and the dynamic range of the signal can easily be seen to have grown rapidly. The lower chart contains the later portion of the F8D track, recorded at a low signal processor level to avoid saturation. During this later period, as the formation passed through the backscatter peak, the typical 30- to 40-db signal dynamic range and focusing-associated peaks in excess of  $20 \mu\text{v}$  p-p were displayed.

Figure 24(b) contains a single extended chart of signal amplitude and apparent radar cross section recorded at an intermediate signal processor level for a two-aircraft formation of F8D interceptors which passed through approximately the same range interval at a later time. The integrated noise level in Fig. 23(b) is approximately  $0.1 \mu\text{v}$  p-p once more, although the later part of the record, at periods after 1200 EST, is contaminated by interference. The large spread peak at approximately 1203 EST is due exclusively to this interference, but all other peaks are associated with the two-aircraft echo. Notice in Fig. 24(b), as in Fig. 24(a), that the low initial signal corresponding to the target's approach through the tail of the backscatter distribution is replaced by an extremely high, deeply fading echo in the range interval around 900 naut mi. Notice also that the two-aircraft echo appears to fade more deeply than the four-aircraft signal and,

in fact, displays a character much like the single-aircraft data presented above. Its focusing-associated peaks also are substantially smaller than those associated with the four-aircraft track, reaching a maximum amplitude of  $10\ \mu\text{V}$  p-p (not shown in Fig. 24(b) due to signal processor and recorder saturation). A great deal of caution should be exercised in drawing general conclusions from these limited data, however, for in the 1-hr period which intervened between them, substantial changes in the (midday) ionosphere could have taken place. Indeed, a 50-mi displacement of the range at which the peak signal was received can easily be seen to have occurred during this interval.

Figure 24(c) contains similar data from one of the air rescue aircraft which was associated with the F8D flights and was tracked through the same approximate range interval at approximately the same time as the two-aircraft F8D formation. A similar signal-amplitude scale to that in Fig. 24(b) is used in Fig. 24(c) for comparison. The same interference peak that affected the two-aircraft track may be seen to appear after 1200 EST in this record as well. The principal feature of Fig. 24(c) is the target's repeated fading to below the  $0.1\text{-}\mu\text{V}$  p-p integrated noise level, even in its passage through the backscatter peak in the 1130 to 1150 EST time interval. The two-aircraft record in Fig. 24(b) may be seen to remain slightly above the threshold level (which was coincident in this case with the integrated noise level) after 1140 EST, although the entrance of an interfering station at around 1200 EST tends to confuse this circumstance somewhat. The single-aircraft echo can also be seen to reach a maximum level of only  $6\ \mu\text{V}$  p-p, as opposed to the  $10\text{-}\mu\text{V}$  p-p level achieved by the two-aircraft target and the  $25\text{-}\mu\text{V}$  level achieved by the four-aircraft signal. Once more, however, the brevity of this statistical sample should impose a note of caution in drawing conclusions from these data alone.

One general statement which can be made with some conviction is that the fading pattern followed by multiple-aircraft targets appears to be different from that followed by single-aircraft targets and tends, specifically, to display less frequent fading nulls to below the integrated noise level. This circumstance suggests that the dominant fading phenomenon is probably one which differentiates between a single aircraft on the one hand, and a closely spaced group of aircraft, spread apart by a few wavelengths and probably varying somewhat in separation, on the other hand. Perhaps, then, the polarization-rotation type of fading which occurs solely within the ionosphere, and hence does not differentiate between these two types of target, is less important as a contributor to the fading than is the interference-type fading. This latter effect, ascribed to a multiplicity of propagation paths between target and radar, would indeed tend to treat a group of aircraft separated by a varying space of a few wavelengths differently from a single aircraft.

In view of the comprehensive character of this section, a brief listing of the primary conclusions seems to be warranted:

- a. A typical OTH aircraft target in the 800- to 2000-naut-mi range interval displays a mean apparent radar cross section of 50 to 200  $\text{m}^2$ .
- b. Such a target can normally be acquired by an OTH radar, which possesses the sensitivity of the Madre radar, on an average of 60 percent of the time during which it is illuminated. (This statement refers to acquirable targets only and no inference should be made to abnormal ionospheric conditions when it is physically impossible to illuminate the target.)
- c. An OTH aircraft target displays a dynamic range in signal amplitude, ranging from the effective noise level to signal amplitude peaks, which can exceed 40 db under circumstances of substantial focusing in the propagation path.

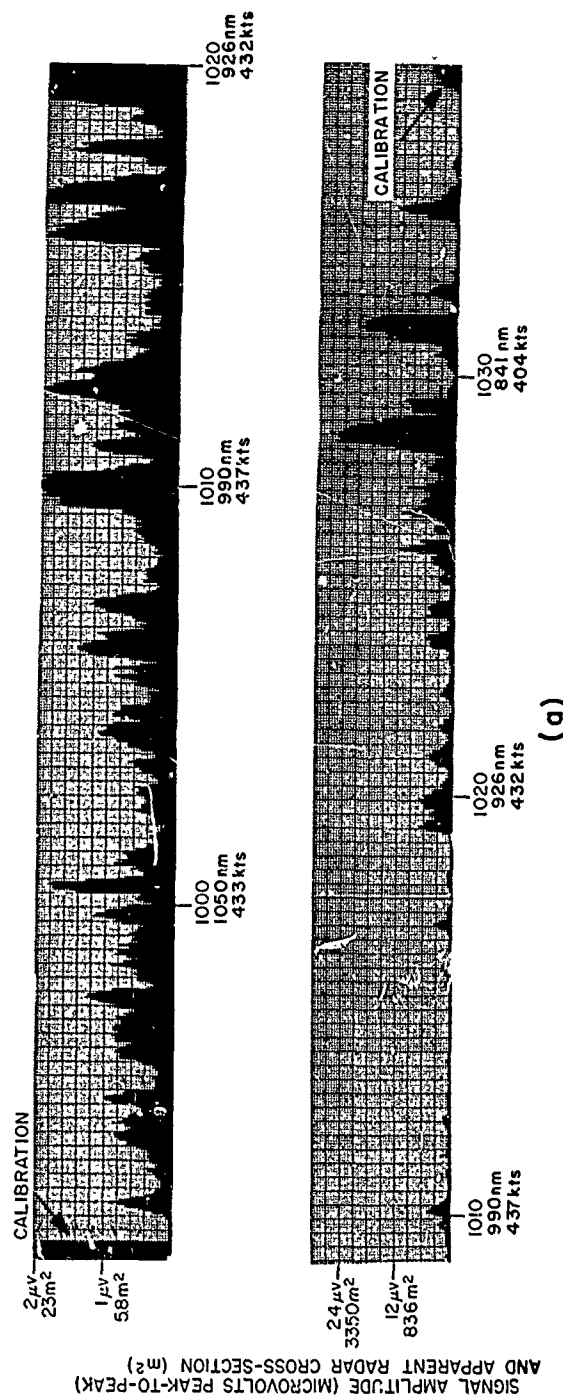


Fig. 24 - Signal amplitude, or apparent radar cross section, for (a) four-aircraft  
(Trojan Queen I) F8D formation, measured on May 15, 1964



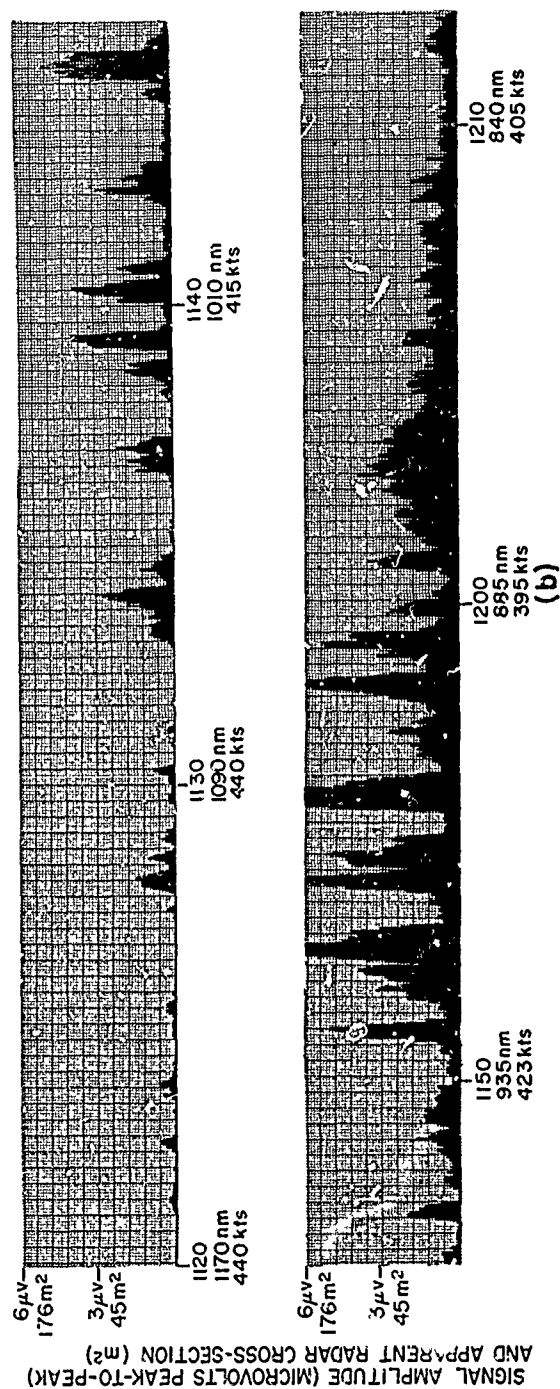


Fig. 24 (cont'd) - Signal amplitude, or apparent radar cross section, for (b) two-aircraft  
(Trojan Queen II) F8D formation, measured on May 15, 1964

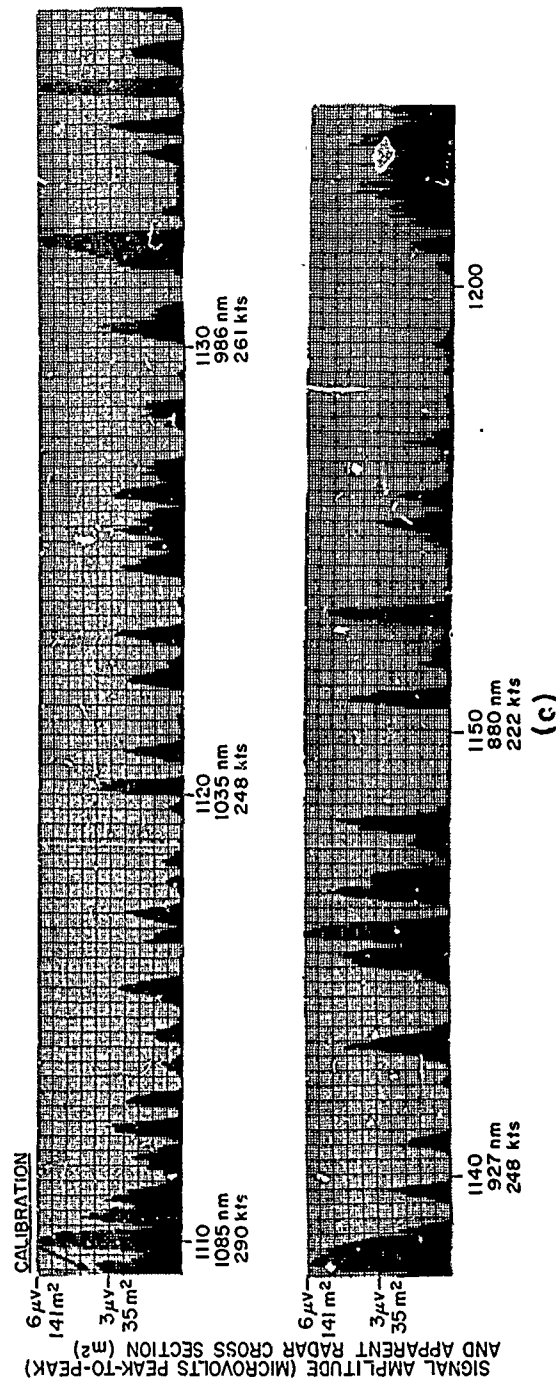


Fig. 24 (cont'd) - Signal amplitude, or apparent radar cross section, for  
(c) single air rescue aircraft, measured on May 15, 1964

d. A noncoherent radar, possessing power and antenna gain characteristics similar to Madre, can probably acquire an OTH aircraft target under these circumstances approximately 6 percent of the time during which it illuminates such a target. Even then, such a radar can provide this degree of sensitivity only if the considerable signal-to-clutter ratio difficulties with which it is beset can be solved.

e. Signal-to-clutter ratios can be expected to vary from below -100 db to as high as -50 db for normal OTH aircraft tracking operations; this range shows no apparent dependence upon the region in the backscatter distribution through which the target is tracked. It should be acknowledged, however, that occasions have occurred on which strong aircraft echoes have been observed from regions in which backscatter coverage has been quite small. These occasions have arisen only infrequently, and it is not believed that the fortuitous circumstances which engender them will permit an operator to cover any desired range interval by this means.

f. Closely spaced groups of targets, separated by a few (varying) wavelengths, display somewhat shallower fading nulls than single-aircraft targets and possibly display a tendency to experience fading peaks with an amplitude proportional to their number.

#### THE SPECTRAL CHARACTERISTICS OF OTH AIRCRAFT RADAR ECHOES

The coherent MTI signal-processing technique which is utilized to provide the 1/10-cps doppler resolution of the Madre analysis system adapts itself readily to a detailed study of the spectral characteristic possessed by selected targets. As has been mentioned in the Introduction to this report, one format in which radar data has been displayed is a linear signal-amplitude vs doppler frequency display which permits an investigation to be made of fine-structure variations in doppler frequency stability of radar targets.

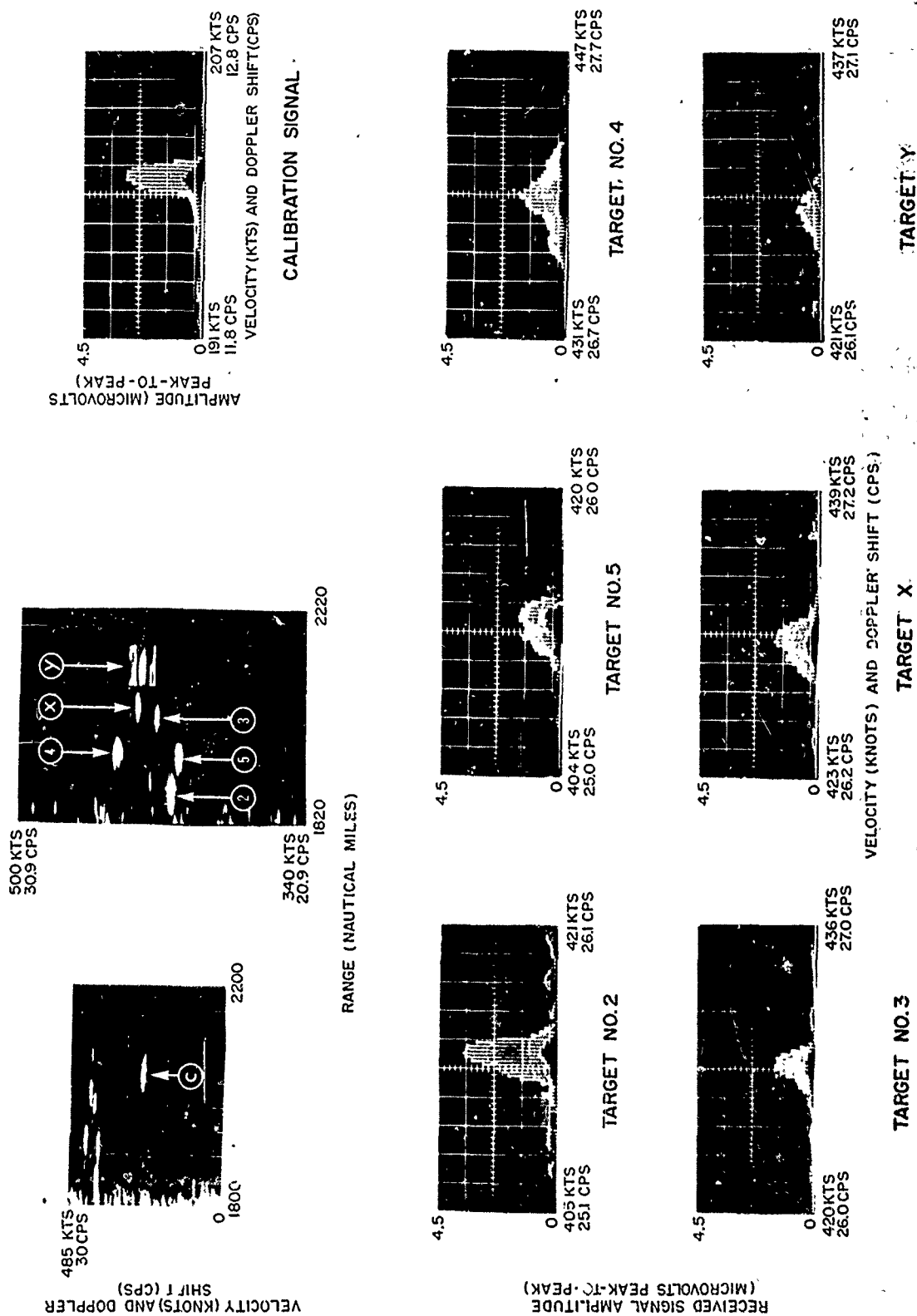
Figure 25 contains a group of photographs which illustrate the spectrum analysis and demonstrate some typical doppler frequency characteristics of OTH aircraft. The photograph in the upper left corner of Fig. 25 is a usual Madre intensity-modulated velocity vs range display showing six strong aircraft echoes clustered near 400 knots (25 cps) in doppler frequency, and spread throughout the 1800- to 2100-naut-mi range interval. A band of system-associated noise also appears along the left side of this photograph, plus a calibration signal trace identifiable by the circled C. The center photograph in the top row is an expanded-doppler view of only 10 cps of the available doppler spectrum, displaying the six targets at a doppler resolution of 1/10 cps. The circled numerals identify four of the targets (targets 2-5) which were observed on Oct. 27, 1964, and were discussed in the previous two sections of this report, plus two additional targets (targets X and Y) which were present only weakly and sporadically and are assumed to have been targets which passed through the extreme edge of the antenna beam. No attempt has been made to identify these latter targets. Target Y may be seen in this photograph to be enclosed in an illuminated window. The window represents the location of the doppler-range gate which is used to study selected targets and, in this case, extends over a range interval of 100 naut mi and a doppler interval of 1 cps (16 kts). The remaining photographs are amplitude vs doppler frequency spectrum analyses which were obtained by placing the doppler-range gate separately on each of the six targets and the calibration signal. The upper right photograph is a spectrum analysis of the calibration signal, which is an effective stable-doppler target and, hence, permits the maximum achievable doppler resolution to be displayed. Its spectrum may easily be seen in this photograph to be approximately 1/10-cps (1.6-kts) wide at the -10-db points,

and this width thus is designated as the resolution limit of the analysis filter. It should be reemphasized that only the envelope of the spectrum displayed in this photograph (and in all others to follow) conveys meaningful information. The spacing of the individual lines within the envelope is related to an arbitrary sampling rate and has no bearing on this discussion.

The bottom two rows of photographs in Fig. 25 are similar spectrum analyses of the six targets; they display the typical behavior of OTH aircraft echoes. Notice that at the time these photographs were taken, targets 2 and 3 possessed rather compressed spectral distributions, extending over approximately 0.15 cps (2.4 kts) in doppler frequency, while Target 4 was spread over nearly 0.4 cps (6.4 kts). The spread-spectrum behavior displayed in this photograph by Target 4 could arise from slight speed adjustments, turns, or changes in altitude of the aircraft during the 20-sec period in which storage of the information, from which the spectrum analysis was made, took place. Over-the-horizon aircraft echoes normally display a spectrum which is most often compressed to within a 1/10- or 2/10-cps band, but which occasionally spreads to as much as 1/2 cps. It should be mentioned that normal ionospheric processes can probably bring about spreading and shifting in the aircraft target spectrum. It is believed that the ionospheric changes, from which these phenomena result, are so gradual as to be undetected by the Madre spectrum analysis.

The temporal behavior of a single aircraft traveling with a constant velocity at 2000 naut mi range is exemplified by the series of spectrum analyses in Fig. 26. These illustrations contain spectrum photographs made at approximate 5-sec intervals during the later portion of the P3A flight of May 5, 1964, which was discussed in the previous two sections of this report. In these photographs, a doppler-range gate of 2 cps  $\times$  100 naut mi was used, and the 1/10-cps doppler resolution corresponded to 1.6 knots. Time (EST) appears below each photograph. The upper left photograph in Fig. 26 contains a spectrum analysis of the calibration signal, although in this case a substantial amount of noise was present near the calibration signal trace and caused its spectrum to be spread somewhat beyond the true resolution limit of the analysis filter. In Fig. 26, in fact, the aircraft echo may be seen to display even better apparent doppler stability than the calibration signal due to the noise-associated spreading of the latter's spectrum. The individual spectrum photographs in Fig. 26, which are for a single-aircraft target traveling at a speed which was known to be relatively constant, give a good indication of the truly fine doppler resolution which is achievable with coherent MTI processing. The single discrete spectral component may be seen to remain compressed in doppler extent and to experience the clear deep fading pattern which was indicated in the previous section as typical of single-aircraft echoes.

The striking difference between the behavior of these single-aircraft doppler spectra and that associated with groups of closely spaced aircraft formations can be seen by comparing Fig. 26 with similar data obtained during the four-aircraft F8D flight of May 15, 1964, which was treated in the previous two sections of this report. Figure 27 contains spectrum photographs which were made with a similar 2 cps  $\times$  100 naut mi doppler-range gate during the four-aircraft F8D flight, and the 1/10-cps doppler resolution corresponds to 1.8 kts at the frequency which was utilized for these observations. Once again, the calibration signal spectrum appears at top left in Fig. 27 and indicates the resolution limit of the analysis filter for the F8D observations. Throughout the series of photographs in Fig. 27, it should be evident that there is a multiplicity of contributors to the total spectrum and that the individual contributors are separated in doppler frequency by a varying amount, spread over somewhat more than 1 cps. Individual aircraft can be picked out in many of the spectrum photographs, particularly those taken between 1026:16 and 1026:33 EST, and also those taken between 1027:55 and 1028:28 EST. It should be apparent from this series of photographs that formations of aircraft can readily be distinguished.



OCTOBER 27, 1964, 1424 EST

Fig. 25 - Velocity vs range and spectrum photographs for selected OTH aircraft target of Oct. 27, 1964

SECRET

NAVAL RESEARCH LABORATORY

47

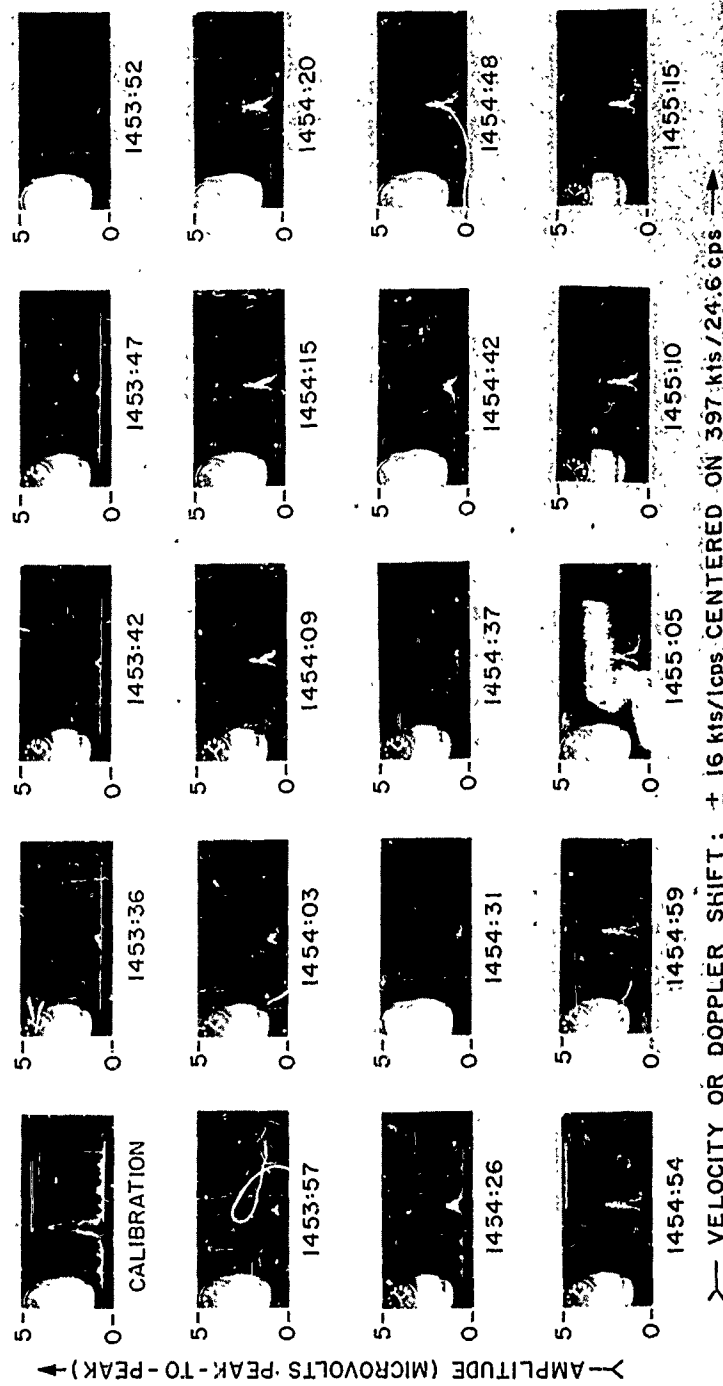


Fig. 26 - Spectrum photographs of a single OTH P3A aircraft, observed on May 5, 1964

SECRET

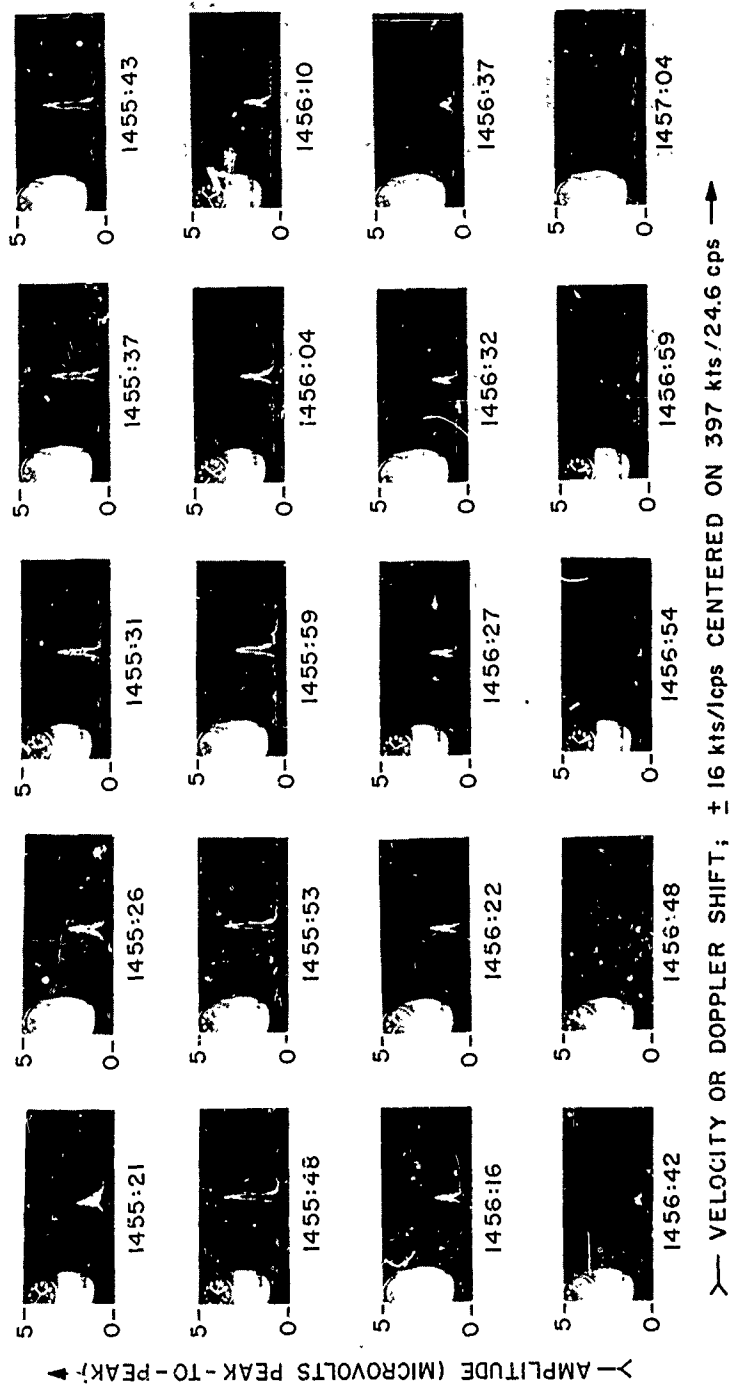


Fig. 26 (cont'd) - Spectrum photographs of a single OTH P3A aircraft, observed on May 5, 1964

from single-aircraft echoes. Indeed, even from this brief series, extending over less than 4 min in time, it is possible to make an estimate of the actual number of aircraft in the formation. One possible explanation of the extreme variability among the photographs of Fig. 27, as compared to those in Fig. 26, is that in the former case the pilots were likely to make more frequent adjustments in speed, heading, and altitude in performing their station-keeping tasks, and hence tended to cause much more frequent shifting and spreading in the spectral distributions of each individual echo.

An additional feature of Fig. 27 is that, in distinction from single-aircraft spectra, there is only a slight tendency for the echoes from individual aircrafts to fade in concert. Instead, most spectral components tend to fade independently of the others, and a substantial amount of energy remains within the doppler-range gate nearly continuously.

A listing of the principal conclusions which can be drawn from this section is as follows:

- a. The ionospheric propagation path will normally permit velocity measurements to be made on OTH aircraft targets with a resolution of at least 1/10 cps in doppler.
- b. This doppler resolution may be utilized to separate individual targets in a closely spaced group (or formation) of aircraft which are too close together to be separated by the range resolution afforded by the radar's pulse length.
- c. The spectral behavior of a multiple-aircraft echo permits an estimate to be made of the actual number of aircraft in such a formation.

## CONCLUSIONS

Each of the three principal phases of the over-the-horizon (OTH) aircraft target study conducted by NRL has given rise to its own distinct conclusions.

For the tracking phase, treated in the second section of this report titled "Time-Range Tracking of OTH Aircraft Targets," these conclusions may be summarized as follows:

- a. It has been possible, under normal-to-good propagation conditions, to track selected aircraft targets almost continuously from ranges of 700 to 2300 naut mi. Such tracks have been acquired with a radar which possesses limited flexibility in frequency and radiation pattern control.
- b. A range measurement accuracy of approximately 5 percent may be expected under usual conditions, even if no effort is made to correct raw slant-range data for effects of the ionospheric path.
- c. Corrections to raw slant-range radar data, which can be made with even the simplest vertical ionospheric sounding data, can contribute significantly to reducing this measurement error.
- d. Operation of an OTH radar in a "fence-crossing" surveillance mode can be expected, under normal-to-good propagation conditions, to provide complete detection data and high-quality range and radial velocity (tracking) data on all aircraft targets within the desired surveillance region. Useful coverage of adjacent, azimuthally displaced regions also is often possible and can, in fact, present a difficulty in target identification due to its effect of increasing the total target population.



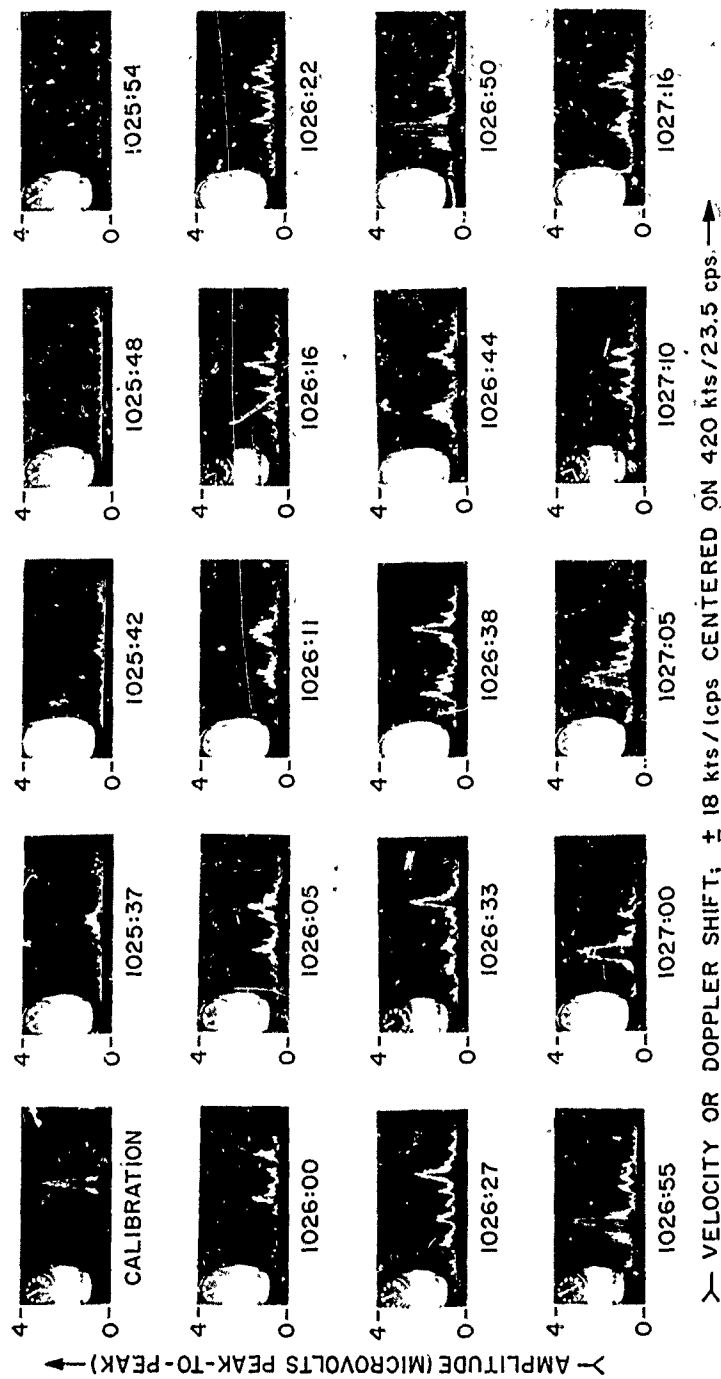


Fig. 27 - Spectrum photographs of four OTH F8D aircraft (Trojan Queen I formation), observed on May 15, 1964

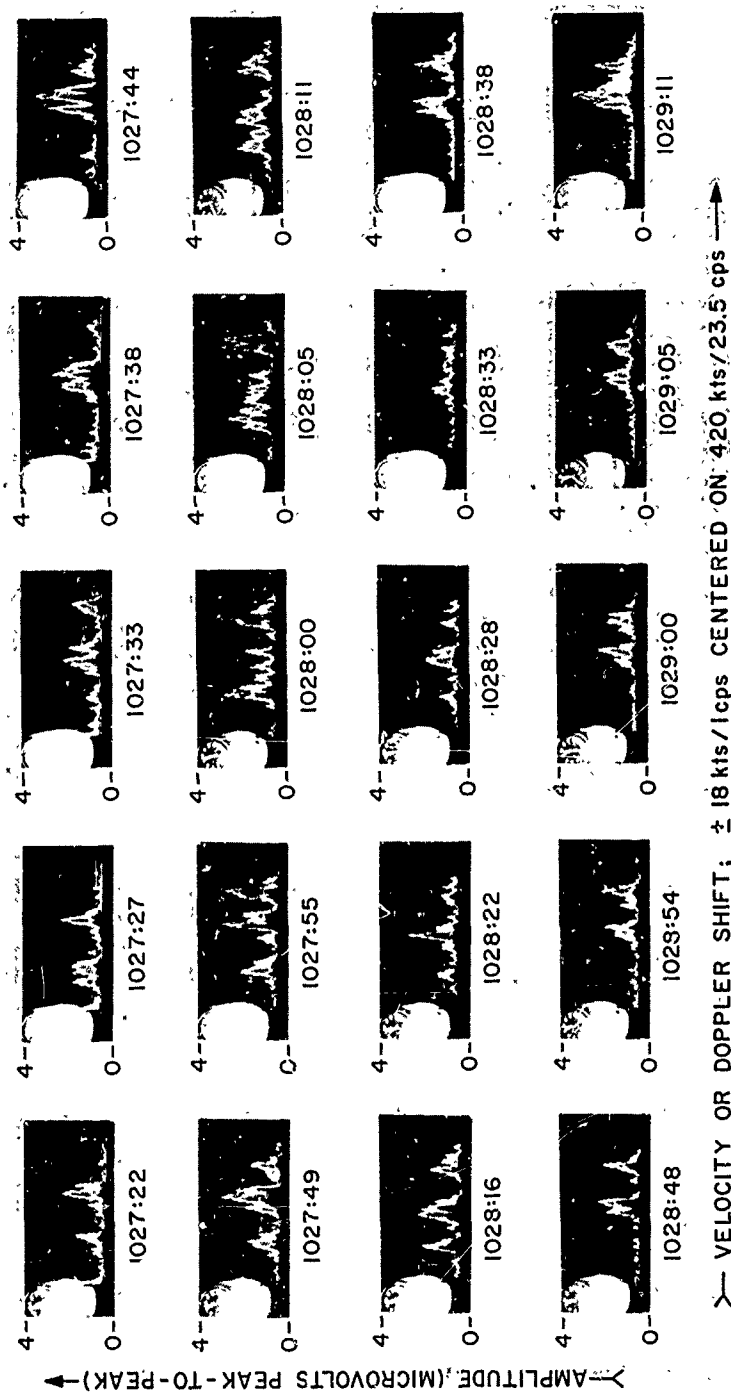


Fig. 27 (cont'd) - Spectrum photographs of four OTH F8D aircraft (Trojan Queen Information), observed on May 15, 1964

The significance of the temporal behavior of the radar echoes, treated in the third section of this report titled "Temporal Variation in Signal Strength of OTH Aircraft Radar Echoes," has been discussed at the end of that section, and the list of conclusions is repeated below:

- a. A typical OTH aircraft target in the 800- to 2000-naut-mi range interval displays a mean apparent radar cross section of 50 to 200 m<sup>2</sup>.
- b. Such a target can normally be acquired by an OTH radar, which possesses the sensitivity of the Madre radar, on an average of 60 percent of the time during which it is illuminated.
- c. An OTH aircraft target displays a dynamic range in signal amplitude, ranging from the effective noise level to signal amplitude peaks, which can exceed 40 db under circumstances of substantial focusing in the propagation path.
- d. A noncoherent radar, possessing power and antenna gain characteristics similar to Madre, can probably acquire an OTH aircraft target under these circumstances approximately 6 percent of the time during which it illuminates such a target. Even then, such a radar can provide this degree of sensitivity only if the considerable signal-to-clutter ratio difficulties with which it is beset can be solved.
- e. Signal-to-clutter ratios can be expected to vary from below -100 db to as high as -50 db for normal OTH aircraft tracking operations; this range shows no apparent dependence upon the region in the backscatter distribution through which the target is tracked. It should be acknowledged, however, that occasions have occurred on which strong aircraft echoes have been observed from regions in which backscatter coverage has been quite small. These occasions have arisen only infrequently and it is not believed that the fortuitous circumstances which engender them will permit an operator to cover any desired range interval by this means.
- f. Closely spaced groups of targets, separated by a few (varying) wavelengths, display somewhat shallower fading nulls than single-aircraft targets and possibly display a tendency to experience fading peaks with an amplitude proportional to their number.

A list of conclusions regarding the spectral behavior of the radar echoes, treated in the fourth section of this report titled "The Spectral Characteristics of OTH Aircraft Radar Echoes," appeared at the end of that section, and the list is reproduced below:

- a. The ionospheric propagation path will normally permit velocity measurements to be made on OTH aircraft targets with a resolution of at least 1/10 cps in doppler.
- b. This doppler resolution may be utilized to separate individual targets in a closely spaced group (or formation) of aircraft which are too close together to be separated by the range resolution afforded by the radar's pulse length.
- c. The spectral behavior of a multiple-aircraft echo permits an estimate to be made of the actual number of aircraft in such a formation.

It should be emphasized that although this report has contained detailed analyses of only a few selected OTH aircraft tracks, its conclusions have been based on a comprehensive catalog of similar data which have been acquired over a four-year period. The particular tracks which have been selected for analysis in this report have been so selected because they represent typical expected behavior under normal-to-good operating conditions. An evaluation of the effects of ionospheric variability upon the performance of the Madre radar is planned as part of NRL's future investigations.

SECRET

#### REFERENCES

1. Page, R.M., "Storage Radar," NRL Report 3532 (Secret Report, Unclassified Title), Oct. 1949
2. Page, R.M., and George, S.F., "Magnetic Drum Storage Applied to Surveillance Radar," NRL Report 4878 (Confidential Report, Unclassified Title), Jan. 1957
3. Wyman, F.E., and Zettle, E.N., "Magnetic Drum Storage Cross Correlation Radar," NRL Report 5023 (Secret Report, Unclassified Title), Nov. 1957
4. McGeogh, J.E., Jensen, G.K., and Uniacke, C.L., "A 100-kc Quartz Crystal Comb Rejection Filter," NRL Report 5589 (Confidential Report, Unclassified Title), Feb. 1961
5. Boyd, F.E., and Rohlf, D.C., "A Very High Power Frequency Pulse Transmitter and Antennas," NRL Report 5903 (Secret Report, Unclassified Title), May 1963
6. Davis, J.R., Headrick, J.M., and Page, I.H., "A System for the Extension of Unambiguous Radar Without Degradation of Velocity Information," NRL Report 5849 (Secret Report, Unclassified Title), Oct. 1962
7. Davis, J.R., "Range Ambiguity Reduction in the MADRE Radar," NRL Memorandum Report 1444 (Secret Report, Unclassified Title), July 1963
8. Davis, J.R., "Range Ambiguity Reduction in the MADRE Radar, Part II - Initial System Evaluation," NRL Memorandum Report 1500 (Secret Report, Unclassified Title), Jan. 1964
9. Davis, J.R., and Headrick, J.M., "Reduction of Range Ambiguity in the MADRE Radar," NRL Report 6148 (Secret Report, Unclassified Title), Nov. 1964
10. Gager, F.M., Headrick, W.C., Morgan, G.A., Utley, F.H., and Zettle, E.N., "MADRE Performance, Part 1 - Very Long Range, Over-the-Horizon Detection of Aircraft with the MADRE Radar," NRL Report 5862 (Secret Report, Secret Title), Dec. 1962
11. Gager, F.M., Headrick, W.C., Morgan, G.A., Rohlf, D.C., Tesauro, C.B., and Zettle, E.N., "MADRE Performance, Part 2 - Observations of Feb. 8, 1962," (Unclassified Title), "MADRE Performance, Part 2 - Very Long Range, Over-the-Horizon Detection of Aircraft with the MADRE Radar," (Secret Title), NRL Report 5898 (Secret Report), Feb. 1963
12. Gager, F.M., Morgan, G.A., Tesauro, C.B., Skaggs, G.A., and Zettle, E.N., "MADRE Performance, Part 3 - Observations of Feb. 12, 1962," (Unclassified Title), "MADRE Performance, Part 3 - Very Long Range, Over-the-Horizon Detection of Aircraft with the MADRE Radar," (Secret Title), NRL Report 5991 (Secret Report), Aug. 1963
13. Gager, F.M., Morgan, G.A., Headrick, W.C., Tesauro, C.B., and Zettle, E.N., "MADRE Performance, Part 4 - Observations of Feb. 15, 1962," (Unclassified Title), "MADRE Performance, Part 4 - Very Long Range, Over-the-Horizon Detection of Aircraft with the MADRE Radar," (Secret Title), NRL Report 6019 (Secret Report), Jan. 1964

SECRET

14. Davis, J.R., Gager, F.M., Headrick, J.M., and Zettle, E.N., with Appendices by Ahearn, J.L., Headrick, W.C., Utley, F.H., Tesauero, C.B., and Ward, E.W., "Information on Over-the-Horizon Radar; Part III," NRL Memorandum Report 1540 (Secret Report, Unclassified Title), June 1964
15. Ahearn, J.L., Headrick, W.C., Headrick, J.M., Tesauero, C.B., and Zettle, E.N., "Extended-Range Aircraft Tracking," NRL Report 6272 (Secret Report, Unclassified Title), May 1965
16. Davis, J.R., Rohlf, D.C., Skaggs, G.A., and Joss, J.W., "Decameter-Wave Studies of the Lunar Surface," Radioscience, 69D(No. 12) (to be published)
17. Tveten, L.H., "High Frequency Propagation Backscatter and Phase Studies," NBS Report 7615, Oct. 1962.
18. Tveten, L.H., "High Frequency Backscatter Studies," NBS System 760B, Project 5582, Task 558203, March 1965

SECRET

## APPENDIX A

### AUTOMATIC DATA-PROCESSING METHODS USED FOR MADRE OTH AIRCRAFT OBSERVATIONS

#### DATA CONVERSION

The data reduction is performed on NRL's NAREC computer, utilizing programs written in the NELIAC-IV language. Before the information punched on paper tape can be used, it is converted by a translation routine into the number system used by the NAREC computer. At the same time, a proof copy is made and is checked for errors before the main data reduction program is begun.

In the meantime, hourly ionospheric scalings are gathered and prepared on punched tape. As of the present, this information is received in the form of graphical scaling data from the National Bureau of Standards' Ft. Belvoir Station. Punched tapes are made from these scalings with the use of a Flexowriter coded for the Control Data G-15 computer, and these tapes in turn are translated in a similar manner to the radar data.

Upon completion of the data conversion phase, the taped information shown in Table A1 is ready for input to the main data reduction program. It is possible to process 740 data points on one tape; this limit is determined by the memory capacity of the computer.

Table A1  
Contents of Punched-Tape Input for  
Data Reduction Program

Observational Radar Data:	
1.	Time of observation
2.	Slant range to target
3.	Range rate of target
4.	Azimuth to target
5.	Radar frequency
Ionospheric Data:	
1.	Time of observation at sounder
2.	Critical frequency, $F_2$ layer
3.	M3000 factor, $F_2$ layer
4.	Minimum height, $F_2$ layer
5.	Minimum height, $F_1$ layer
6.	Critical frequency, $F_1$ layer
7.	M3000 factor, $F_1$ layer
8.	Critical frequency, $E$ layer (not used)
9.	Minimum height, $E$ layer
10.	$f_o E_s$ (not used)
11.	Critical frequency, $E_s$ layer (not used)
12.	Minimum height, $E_s$ layer (not used)

SECRET

## DATA REDUCTION

In performing the ionosphere analysis phase of the data reduction program, it is assumed that all paths are single hop. The ionospheric reflection point is undetermined, variable, and over the ocean, and hence it is impractical to obtain vertical soundings. For this reason, the sounding data are taken from the nearest ionospheric sounding station (Ft. Belvoir) and extrapolated to the approximate reflection point. In performing this extrapolation, an approximate ground range is computed by subtracting 100 naut mi from the measured target slant range. The longitude of one half of this ground range is computed, using a spherical trigonometric function, and from this longitude the local standard time at the path midpoint is computed. It is then assumed that the ionospheric characteristics "move" with the sun and, hence, will be locally similar for all longitudes (at a given latitude) for the same local time. This method results in a time delay of several hours between the time at which the ionospheric vertical soundings are made, which are used in analyzing the radar data, and when the radar observations themselves are made. When the ionosphere is stable the correspondence is believed to be good, but it is recognized that serious errors can arise if ionospheric disturbances intervene. An additional error due to slight differences in latitude between the sounding station and the radar-wave's ionospheric reflection point is also possible. Provision has been made at this point of the program (in conjunction with later machine decisions) to suppress the computation of paths when it is apparent from the scalings that a layer is incomplete or nonexistent.

In the next part of the program an attempt is made to reconstruct the ionogram from the scaled data by choosing an ellipse which fits the data. (A polynomial curve-fitting program has also been tried and works equally well.) Only the lower right quadrant of the ellipse is used. The ellipse is placed so that the lower side matches the minimum layer height and the right side matches the critical frequency; the ellipticity is empirically related to the 3000-km multiplication factor.

Once the ionogram is reconstructed, a scaling process is started, as follows, to determine the virtual height of reflection of the oblique path:

- a. assume an oblique reflection height  $h'_o$  equal to the minimum layer height  $h'$ ;
- b. compute the angle of incidence for the given slant range and  $h'_o$ ;
- c. solve the secant equation,\* namely,

$$f_{\text{oblique}} = f_{\text{vert.}} \sec \phi$$

where  $f_{\text{oblique}}$  is the radar operating frequency,  $f_{\text{vert.}}$  is the vertical incidence frequency which reflects from the same height, and  $\phi$  is the angle of incidence of  $f_{\text{oblique}}$ ;

- d. using the equation for the simulated ionogram, solve for the vertical reflection height corresponding to  $f_{\text{vert.}}$ ; and

- e. if the difference between the height  $h'_o$  assumed in step a and the vertical reflection height arrived at in step d is less than 5 km, the process is completed; otherwise, 5 km is added to  $h'_o$  and the process is repeated.

\*"Ionospheric Radio Propagation," National Bureau of Standards, Monograph No. 80, pp. 161 and 292.

This process does not often reach a successful conclusion, possibly because the radar is so often operated at a frequency which is very close to, or even above, the maximum usable frequency (MUF) indicated by the vertical soundings. This failing may be attributed mainly to the lack of ionospheric data at the path midpoint and, additionally, to the numerous assumptions it is necessary to make. (It has been shown that very good agreement results when an oblique sounder and a vertical sounder impinge on the same ionospheric area.) In order to continue the program on a "best guess" basis, the following decisions are made:

a. If the equivalent vertical frequency exceeds the critical frequency, the reflection height is made equal to 1.33 times the minimum layer height. This ratio was decided upon after manually scaling a few typical ionograms at the MUF for 600- to 2000-naut-mi ranges. It is only at the very short ranges that the virtual height deviates by a large amount from this value.

b. If the equivalent vertical frequency moves left of the center of the ellipse (i.e., decreases), the height is made equal to the minimum layer height.

In each case a number is printed out under the heading "F HT Method" according to the code shown in Table A2. Heights are computed for each of the following ionospheric layers, if they exist:  $F_2$ ,  $F_1$ ,  $E$ , and  $E_s$ . Simulation and scaling of the ionogram is done only for the two  $F$  layers;  $E$  layer reflections are assumed to always occur at the minimum layer heights. This is nearly always true, and even were it not so, the error is small because of the lower heights involved with the  $E$  layer.

Table A2  
Data Reduction Program Printout Codes

F HF Method:

- 0 - The layer does not exist.
- 1 - Scaling was made from ellipse-simulating ionogram.
- 2 - Height set to 1.33 times minimum height because program unable to complete when  $F_{\text{vert.}} > f_o$ .
- 3 - Height set equal to minimum height because  $F_{\text{vert.}}$  is on zero slope (low-frequency part) of simulated ionogram, or  $f_o$  is not given (i.e.,  $F_o = 0$  in table).

MUF:

- 0.1 - The layer height is not given.
- 0.2 - The ground range exceeds 2150 naut mi.
- 0.3 - The critical frequency is not given.

Plotter Symbols:

- (circle) -  $F_2$  layer.
- (square) -  $F$  layer.
- ◇ (diamond) -  $E$  layer.
- ◻ (quarter circle) -  $E_s$  layer.
- ⊙ (hexagonal) - Margin marks.



Once the reflection heights have been determined, an accurate computation of the target ground range, latitude and longitude, and angle of arrival is completed using the spherical trigonometric function once more. Range rate (which is read in terms of doppler frequency) is corrected for (a) radar frequency, and (b) angle of arrival. The MUF's of the *F* layers are computed using a computer-adapted version of the nomogram method shown in Ref. 19. Any unrealistic MUF's which may be printed out have three possible meanings, as shown under "MUF" in Table A2. The ratio of operating frequency to MUF is computed and printed, and departure angles for all possible modes are printed out to help the observer to determine which layer is the most probable one used. (See Appendix B for a discussion of selection of the most probable mode.) The final computation converts accuracy in azimuth to a linear distance in naut. mi. For this computation the target is assumed to fall within the  $\pm 3$ -db power points of the antenna beam. The correct beamwidth is extracted from a table of beamwidth vs frequency using a linear interpolation subroutine. The azimuth uncertainty formula is as follows:

$$\text{azimuth uncertainty} = (\text{antenna beamwidth}) \times (\text{ground range}).$$

#### DATA PRESENTATION

A typical printout of the computed data is shown in Table A3. The heights printed are the ones determined by the program and used in the calculations. Time and slant range are the only input data printed out. In addition to the hard copy, the computer produces a tape containing the time and various ground ranges for each data point. When this tape is run on a data plotter, it produces a range vs time plot, such as that shown in Fig. 10 in the text.

Table A3  
Typical Printout of Computer-Reduced Data Point

TIME (GMT)	19: 17	RANGE R E (K.)	*****
MIDPOINT LST	15.30	RANGE R ES (K.)	*****
SLANT R (N.MI.)	1667.	DEPART DEG. F2	11.7
HEIGHT F2 (KM.)	482.	DEPART DEG. F	3.3
HEIGHT F (KM.)	270.	DEPART DEG. E	*****
HEIGHT E (KM.)	103.	DEPART DEG. ES	*****
HEIGHT ES (KM.)	.	F2MUF	14.7
GND R F2 (N.MI.)	1530.	OP FREQ/F2MUF	1.22
GND R F (N.MI.)	1611.	F1MUF	15.0
GND R E (N.MI.)	.	OP FREQ/F1MUF	1.20
GND R ES (N.MI.)	.	AMBIGUITY F2	296.
POSITION F2	40 36N 43 16W	AMBIGUITY F	312.
POSITION F	40 26N 41 30W	AMBIGUITY E	*****
POSITION E	*****N*****W	AMBIGUITY ES	*****
POSITION ES	*****N*****W	F2 HT METHOD	2
RANGE R F2 (K.)	404.	F HT METHOD	2
RANGE R F1 (K.)	396.		

SECRET

## APPENDIX B

### SELECTION OF MOST PROBABLE IONOSPHERIC PATH

In order to most accurately determine the ground range on over-the-horizon radar targets in which the ionosphere is used as a reflecting medium, an accurate assessment of the reflection height must be made. Through the use of the digital computer routine discussed in Appendix A, NRL's NAREC computer is programmed to determine a reflection height and corresponding target ground ranges for each of the usable ionospheric layers. Depending on ionospheric conditions, there may be as many as four effective reflection layers, resulting in four possible ground ranges for each slant-range radar point. (Only single-hop paths are considered.) To obtain maximum utility from the radar, it is advantageous to determine which of the possible paths is in use for each observation. (Nominal range accuracy obtained without this path assessment is normally 5 percent.) If for a single target there exists only one radar-range velocity trace position, a simple process of selecting the lowest attenuation path predicted by the computer will permit a reasonable estimate of the path in use. However, even if the antenna pattern of the radar and the effective scattering pattern for the target (as a reflector above ground) are known sufficiently accurately, the task of obtaining detailed ionospheric information and calculating this path attenuation is extremely difficult. Another possible approach to this problem is to provide an antenna with a sufficiently narrow elevation antenna pattern to effectively select a desired departure angle (and hence the mode). However, since neither of these methods of mode selection is feasible with the equipment presently available, a more qualitative, and somewhat less accurate, method is currently being used.

Table A3 in Appendix A shows typical computer output data for the P3A flight of May 5, 1964, discussed in the second, third, and fourth sections of this report. It is apparent from this computer data that there are only two possible propagation paths, and the  $E$  and sporadic- $E$  layers are either nonexistent or too low in altitude to support propagation to the ranges involved. At 1917 GMT (1417 EST) the measured slant range (radar range) is 1667 naut mi. The maximum usable frequency (MUF) associated with  $F_2$  propagation at this time is 14.7 Mc/s. The MUF associated with an  $F_1$  mode at this time is 15.0 Mc/s. Because these two MUF's are relatively close together in frequency, additional information is necessary before a decision can be made concerning the actual mode in use. In addition, the calculated MUF for both of the possible layers falls below the operating frequency (18.036 Mc/s), indicating that the available ionospheric data are not sufficiently accurate for this case.

A consideration of the radiation pattern of the Madre broadside array is of some utility in resolving this uncertainty, however. Although this antenna does not have the single, narrow-beam, positionable elevation lobe required for precise mode selection, some information may be gleaned from a knowledge of its elevation pattern and the angles of departure for the various modes. Figure B1 shows the calculated elevation pattern for the broadside array. During the operations of May 5, 1964, the broadside array was utilized in the in-phase mode. (During in-phase operation the two stacked bays of array elements are operated in phase, producing an antenna pattern with relatively good radiation at low angles.) From the computer data in Table A3, the departure angles associated with  $F_2$  and  $F_1$  paths are seen to be 11.7 and 3.3 degrees, respectively. Reference to Fig. B1 indicates that the  $F_2$  path would be attenuated by 12 db (two-way) below the  $F_1$  path

SECRET

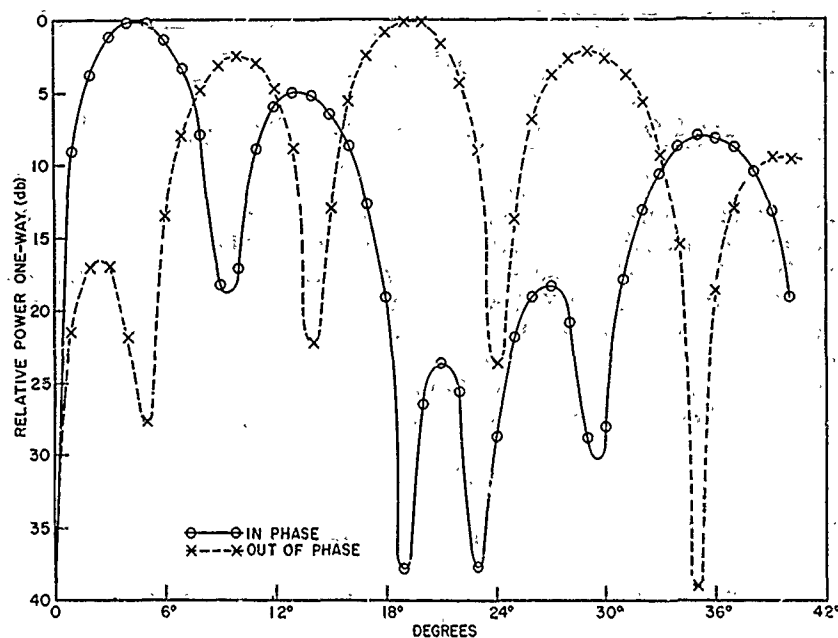


Fig. B1 - Elevation pattern for the Madre broadside array at 18.036 Mc/s. Since the array is broadside, the angles shown are also the angles measured above the horizontal.

on the basis of antenna pattern alone. Due to this fact and to the fact that the  $F_1$  path is slightly preferred on the basis of MUF, the  $F_1$  mode is selected as the most probable mode.

Determining the mode in use for this particular point is relatively straightforward, but in some cases more information may be necessary for isolated point analysis. In dealing with long tracks, however, it is generally possible to find time intervals where the determination of the propagating layer is relatively simple. By extrapolation of the ground-range vs time track and the range-rate vs time tracks in these cases, it is possible to determine the target's range rate and range which would be expected for times at which the effective modes are not so easily determined. Because the range rate and range associated with particular propagation modes are distinct from each other, the layer which, on this basis, yields a range rate and range closest to the observed quantities may be selected as the most probable mode. Shifts from one mode to another may be clearly seen on both the ground-range vs time and the range-rate vs time plots.

# Naval Research Laboratory

## Technical Library

### Research Reports & Bibliography Unit

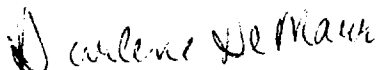
**To:** Larry Downing, DTIC  
**From:** Darlene DeMarr, Code 5596.3  
**Date:** 9/17/2007  
**Subject:** Change in Classification & Distribution Statement

---

Please change the classifications & distribution statement on the following documents to  
Unclassified/Unlimited Distribution:

ADC954564 (NRL-3703-PT-1)	Declassified with no restrictions 9/11/1996
AD0348828 (NRL-6066)	Declassified with no restrictions 9/30/1996
AD0348901 (NRL-6037)	Declassified with no restrictions 12/3/1996
AD0352827 (NRL-6117)	Declassified with no restrictions 1/25/1996
AD0361630 (NRL-6247)	Declassified with no restrictions 1/7/1997
AD0377010 (NRL-6476)	Declassified with no restrictions 1/29/1997
AD0377011 (NRL-6485)	Declassified with no restrictions 1/29/1997
AD0377242 (NRL-6479)	Declassified with no restrictions 1/29/1997
AD0379058 (NRL-6508)	Declassified with no restrictions 1/29/1997
AD0379893 (NRL-6507)	Declassified with no restrictions 1/29/1997
AD0346383 (NRL-6015)	Declassified with no restrictions 1/29/1997
AD0349268 (NRL-6079)	Declassified with no restrictions 1/29/1997
AD0355651 (NRL-6198)	Declassified with no restrictions 1/29/1997
AD0368068 (NRL-6371)	Declassified with no restrictions 1/29/1997

Thank you,



Darlene DeMarr  
(202) 767-7381  
demarr@nrl.navy.mil